

THS

LIBRARY
Michigan State
University

This is to certify that the

thesis entitled

Distribution of Ventilation in Anesthetized Horses

presented by

Paul R. Sorenson

has been accepted towards fulfillment of the requirements for

M.S. degree in Physiology

Major professor

Date___May 11, 1978

O-7639

DISTRIBUTION OF VENTILATION

IN ANESTHETIZED HORSES

Ву

Paul R. Sorenson

A THESIS

Submitted to
Michigan State University
in partial fulfillment of the requirements
for the degree of

MASTER OF SCIENCE

Department of Physiology

9 112 10x

ABSTRACT

DISTRIBUTION OF VENTILATION IN ANESTHETIZED HORSES

Ву

Paul R. Sorenson

Inhomogeneities of ventilation as they may relate to impaired gas exchange during general anesthesia in the horse were assessed in four body positions, 1) left lateral, 2) right lateral, 3) dorsal, and 4) sternal recumbency, using multiple and single breath N₂ dilution tests. Changes in body position did not shift the distribution of tidal volume between functional lung units. Regional asynchronous ventilation was significantly increased in the lateral and dorsal postures. Vital capacity (VC), expiratory reserve (ER) and functional residual capacity (FRC) were significantly elevated in sternal recumbency, suggesting a reduction in lung elastic recoil. Closing volume (CV) did not change with posture, and exceeded resting lung volume in all body positions except sternal recumbency. Increased lung elastic recoil and reduction in resting lung volume below CV indicate that small airway closure may occur during tidal breathing and be a predominant factor limiting gas exchange in the laterally recumbent anesthetized horse.

ACKNOWLEDGEMENTS

I must extend my appreciation to Dr. N. E. Robinson for his support and guidance throughout this study, and the professional freedom he has extended to me over the past years. I would also like to thank the members of my committee, Doctors L. F. Wolterink and S. R. Heisey. A special appreciation is extended to Dr. Wolterink for his interest and ideas on all phases of my research.

The members of our laboratory are to be acknowledged. I thank

Dr. T. Kozlowski, Roberta Milar, and Lynne Olson for their support and
technical assistance.

A very special acknowledgement is given to all members of the 'Fish lab' past and present, and, in particular, Doctors P. O. Fromm, J. R. Hoffert, H. L. Bergman, R. L. Walker, and Ester Brenke for their continued support over the years. My deepest thanks are expressed to William Jackson for his interest and assistance.

This investigation was supported in part by Grant 1-RO1-HL-17768 from the National Heart and Lung Institute.

TABLE OF CONTENTS

	Page
LIST OF TABLES	iv
LIST OF FIGURES	v
	
INTRODUCTION	1
LITERATURE REVIEW	4
MATERIALS AND METHODS	25
Pressure-volume Experiments	25
Closed Circuit N ₂ Experiments	35
RESULTS	41
DISCUSSION	64
LIST OF REFERENCES	79
APPENDIX	85

LIST OF TABLES

TABLE	Ξ	Page
1.	Lung volumes (liters) determined from quasi-static P-V curves of the lung as a function of body position	44
2.	Values for parameters of the single breath N $_{2}$ washout test in different body positions	47
3.	Estimated functional residual capacity (FRC, liters) given by closed and open circuit N_2 dilution experiments	49
4.	Variance of residuals (measured F_{N_2} - predicted F_{N_2}) X 10 ⁴ for the three basic lung models investigated	55
5.	Estimated compartment volumes and tidal volumes (liters) as a function of position given by the 2 compartment models incorporating deadspace	57
6.	Specific tidal volume (ξ , V'_T/V) predicted from the model parameters using the effective tidal volume ($V'_T = V_T - V_D$) as a function of posture	60

LIST OF FIGURES

FIGUR	E	Page
1.	A hypothetical regional pressure-volume (P-V) curve	11
2.	Four compartmental representations of the lung	16
3.	Schematic representation of the experimental equipment used for simultaneous recording of quasi-static pressure-volume curves and single breath N ₂ washouts	27
4.	Representative recordings of quasi-static lung (P_{TP}) and thoracic (P_{TT}) P-V curves and the single breath N ₂ washout	31
5.	Results of non-linear least squares fit of equation 8	34
6.	Schematic diagram of equipment used to perform closed circuit N ₂ equilibrations	37
7.	Representative recording of fractional N_2 concentration versus time during a closed circuit N_2 equilibration and subsequent open circuit N_2 washin	40
8.	Composite expiratory quasi-static lung P-V curves determined from 8 horses in four body positions	43
9.	Effect of position on the single breath N ₂ washout for one horse	46
10.	Dimensionless N_2 concentration (F'_{N_2}) plotted against breath number (n) for a horse in right lateral recumbency.	54
11.	Mean distributions of specific tidal volume (ξ) given by the model of Gomez for 7 horses in three body positions	59
12.	Estimated subdivisions of lung volume (V) in liters as a function of body position	62

INTRODUCTION

Impairment of gas exchange during general anesthesia has been demonstrated in both man and horse, and is associated with increases in both venous admixture and alveolar-arterial oxygen tension difference (P_{A-aO_2}) (Campbell et al., 1958; Hall et al., 1968). In man, increases in P_{A-aO_2} have been correlated with a reduction in resting lung volume (functional residual capacity, FRC) and an increase in trapped thoracic gas (Don et al., 1972). A reduction in FRC has been demonstrated in the anesthetized horse, and is primarily related to the change in body position; standing versus lateral recumbency (McDonell and Hall, 1974). Further, $P_{A-aO_{2}}$ in both anesthetized horses and man is dependent on the mode of ventilation, with A-a gradients in positive pressure ventilated patients being lower than in spontaneously ventilated patients (Gillespie et al., 1969; Nunn, 1969). The dependence of P_{A-aO_2} on lung volume and mode of ventilation suggests that impaired gas exchange during anesthesia may be the result of increases in regional inhomogeneities of ventilation.

The lung is an elastic structure suspended in the thorax and subject to gravitational forces by virtue of its own mass. Static gravitational stress distributions within the lung result in a vertical gradient of pleural pressure and regional lung volumes, with upper regions, relative to the gravitational field, being more distended than

lower regions (Milic-Emili et al., 1966). Ventilation is preferentially distributed to upper lung units at low lung volumes while lower regions are better ventilated at high lung volumes.

For efficient gas exchange to occur, regional ventilation (V) must match regional blood flow (\mathring{Q}) . The distribution of perfusion is also gravity dependent with higher regions, relative to the gravitational field, being relatively underperfused (Kaneko et al., 1966). Due to these static gravitational influences, the reduction in FRC during anesthesia may cause a shift in ventilation toward upper, poorly perfused lung units, resulting in an increase ventilation-perfusion (V/Q) inequality and elevated P_{A-aO_2} . In addition, there is a critical lung volume at which small airways in lower lung regions may close (closing volume, CV). Airway closure results in a lung region where V/Q=0 contributing to venous admixture. The presence of closed airways during tidal breathing has been implicated as a major factor limiting gas exchange in anesthetized man (Craig et al., 1971B).

Regional distributions of ventilation are dependent on the transmission of forces from the thoracic and abdominal surfaces through the lung parenchyma, and also on local stress distributions between mechanically interdependent lung units (Mead et al., 1970). The change in body position and thoracic muscle tone with anesthesia may alter lung-chest wall interactions and contribute to ventilatory inhomogeneities (Rehder et al., 1977).

The predominant factor influencing regional inhomogeneities of ventilation is the distribution of gravitational stress through the

lung. Because of the large thorax, reorientation of the lung in the gravitational field and the constraints on thoracic and diaphragmatic movement, impaired gas exchange in the anesthetized horse may be attributable to changes in the regional distribution of ventilation and either intermittant or continuous airway closure in dependent lung regions during tidal breathing. This study was designed to assess these factors through the use of multiple and single breath indicator dilution experiments with the application of several mathematical models to describe lung ventilation as a function of body position.

LITERATURE REVIEW

In conscious man, alveolar-arterial oxygen tension difference (P_{A-aO_2}) averages 8 mm Hg with inspired oxygen concentrations of 20-30% $(F_{IO_2}=0.2-0.3)$ (Raine and Bishop, 1963; Mellemgaard, 1966) and increases to approximately 50 mm Hg in anesthetized subjects (Nunn et al., 1965; Bergman, 1967). When $F_{10_2}=1.0$, P_{A-a0_2} increases from 70 mm Hg in conscious subjects to 200 mm Hg following anesthesia, and venous admixture (Q_S/Q_T) increases from 4% to 14% (Nunn, 1964; Mellemgaard, 1966; Bergman, 1967; Marshall et al., 1969). In the horse, PA-aO2 increases from 18 mm Hg in the awake standing animal to 37 mm Hg (F_{10} =0.2) immediately following induction of anesthesia and lateral recumbency (Hall et al., 1968). Alveolar-arterial oxygen tension differences in spontaneously ventilated and positive pressure ventilated horses during halothane anesthesia (F_{10} =1.0) averaged 400 mm Hg and 300 mm Hg respectively with a 14% shunt fraction (Q_S/Q_T) (Hall et al., 1968; Gillespie et al., 1969). The similar magnitudes of P_{A-aO_2} and Q_S/Q_T suggest that the mechanism involved in impaired gas exchange with anesthesia is similar in both man and horse.

Increased P_{A-aO_2} may be the result of 1) impaired alveolocapillary diffusion, 2) mismatching of ventilation (V) and perfusion (Q), or 3) right to left pulmonary vascular shunt. Bergman (1970) demonstrated a significant increase in P_{A-aO_2} with no change in carbon

monoxide diffusing capacity in anesthetized man, indicating that the development of an alveolo-capillary diffusion barrier is not a major factor impairing gas exchange during anesthesia.

In order to determine the relative contribution of V/Q inequalities and right to left shunts to elevated P_{A-aO_2} , P_{A-aO_2} and shunt fraction . . . (Q_S/Q_T) are measured while breathing 100% O_2 . In this case, only regions with V/Q=0 (shunt) contribute to P_{A-aO_2} and are the result of anatomic and physiologic intrapulmonary shunts. Anatomically, venous admixture occurs via arterio-venous anastomoses in the pulmonary circulation and the bronchial and thebesian circulation. Physiologic shunts are due to small airway closure with the subsequent equilibration of trapped alveolar gas with mixed venous blood. The large P_{A-aO_2} seen in both anesthetized man and horse when F_{IO_2} =1.0 indicates a major contribution of intrapulmonary shunting to impaired oxygenation.

To separate the components of intrapulmonary shunting, a solution of a relatively insoluble inert gas is administered intravenously. Because of the low solubility, the inert gas marker evolves rapidly when the blood contacts an airspace, and the concentration of the marker gas in the blood leaving an alveolar capillary is essentially zero. Therefore, any inert gas retained in the arterial blood must have been contributed by blood flow through intrapulmonary arterio-venous anastomoses. Using tritium ($^3\mathrm{H}_2$), Mellemgaard (1966) determined that less than one-third of the 3% shunt fraction in normal man was attributable to arterio-venous anastomoses. Further, there was an age related increase in $\mathrm{P}_{\mathrm{A-aO}_2}$ with no change in blood flow through arterio-venous

anastomoses. While an increase in bronchial and thebesian circulation could account for the increased P_{A-aO_2} , Anthonisen et al. (1969), using a modified single breath N_2 washout maneuver, reported evidence for increases in small airway closure with age. These data suggest that small airway closure is the predominant factor influencing the development of intrapulmonary shunting in normal man.

A common feature of increasing age and general anesthesia is a reduction in resting lung volume (FRC). In man, general anesthesia results in a 44% decrease in FRC. Sixty percent of this reduction in FRC is accounted for by the change from seated to supine posture, with 40% occurring after induction of anesthesia (Craig et al., 1971A,B; Don et al., 1972). At low lung volumes, dependent lung regions may be subject to airway closure (Milic-Emili et al., 1966). When FRC falls below a critical lung volume at which small airways are thought to close (closing volume, CV) there is an increase in P_{A-aO_2} and trapped thoracic gas in both conscious and anesthetized man (Craig et al., 1971B; Don et al., 1972). Wyche et al. (1973) observed that elevating FRC with positive airway pressures can improve arterial oxygenation during anesthesia, presumably by reducing the amount of airway closure. Functional residual capacity is reduced by 50% in the anesthetized horse, primarily as a result of the change in body position (McDonell and Hall, 1974). The relationship of FRC to CV has not been investigated in the horse, and, as in man, may be involved in the increased P_{A-a0} seen with anesthesia.

As inspired oxygen percentage is reduced from 100%, V/Q inequalities start contributing to P_{A-aO_2} , with areas of low V/Q exerting the greatest influence on arterial oxygenation due to the shape of the hemoglobin dissociation curve. The calculation of shunt fraction when $F_{IO_2} < 1.0$ assumes that increased P_{A-aO_2} is solely the result of adding mixed venous blood to ideal arterial blood $(P_{AO_2} = P_{aO_2})$. Increases in shunt fraction as F_{10_2} is reduced from 1.0 reflect an 'as if' shunt resulting from the addition of a component due to areas of low V/Q to the intrapulmonary shunt component. In normal man, $Q_{\rm g}/Q_{\rm m}$ increases from 3% to 5% when F_{10_2} is reduced from 1.0 to 0.2 (Mellemgaard, 1966). Shunt fraction is also increased as alveolar P_{0_2} is reduced during anesthesia (Nunn et al., 1964). The combination of increases in V/Q inequalities and intrapulmonary shunting due to small airway closure are the major determinants of P_{A-aO_a} and venous admixture associated with general anesthesia. Since small airway closure is an extreme form of regional inhomogeneity of ventilation, increases in airway closure and the large shift in resting lung volume during anesthesia suggest that changes in regional ventilation may be the predominant factor determining V/Q inequalities.

Regional inhomogeneities of ventilation have been investigated in man by measuring regional concentrations of an inert gas indicator.

Following inspiration of an inert gas of known concentration, regional inert gas concentration is given by dividing the product of the inspired indicator concentration and the regional inspired volume by the end inspiratory regional volume. Milic-Emili et al. (1966) arranged 12

scintillation counters at various levels behind the thorax of seated men, and recorded regional count rates of Xe introduced in the inspirate. By knowing the inspired and regional 133Xe concentrations. the topographic distribution of regional lung volumes as a function of overall lung volume can be determined. At any given lung volume, apical regions were found to be relatively distended over more basal areas, and ventilation was preferentially distributed to apical units at low lung volumes while basal units were better ventilated at high lung volumes. Topographic distributions of regional volume determined in prone, supine, and laterally recumbent man by the same technique demonstrate that the distribution of regional lung volume is dependent on the orientation of the lung in the gravitational field, with upper (relative to the gravitational field) lung regions always relatively more distended than lower regions (Kaneko et al., 1966). Direct histologic measurement of alveolar size in dog lungs frozen in situ also demonstrates a vertical distribution of volume relative to the gravitational field which can be accentuated by increases in gravitational acceleration (Glazier et al., 1967).

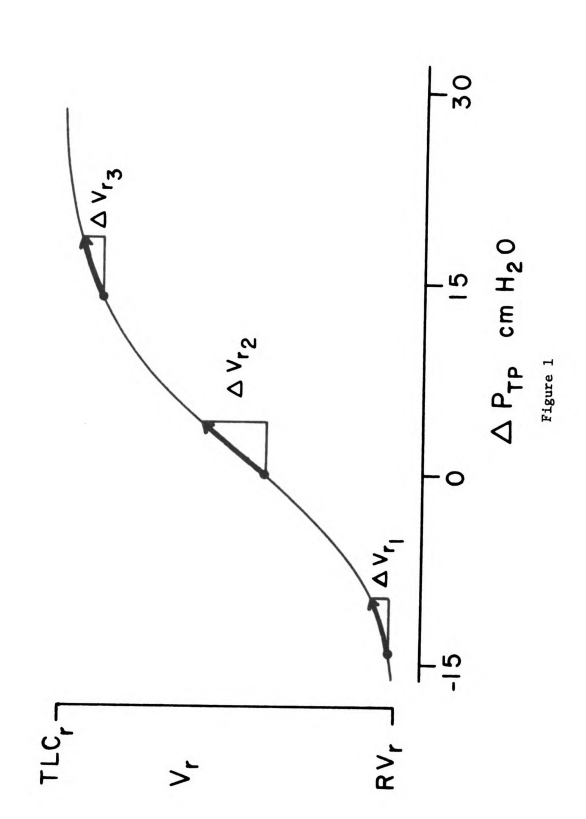
In any plane taken through the lung normal to the gravitational field, alveoli within the plane are subjected to a distending force proportional to the mass of the lung below the plane and the cross sectional area of the lung at this level. By measuring cross sectional area of serial transverse sections and the weight of the lung below each section in a dog lung frozen in situ, Glazier et al. (1967) predicted the regional distending force due to gravity. This regional

distending force correlated well with their determinations of the vertical (relative to the gravitational field) gradient of alveolar size. Since the lung is mechanically interdependent with the thorax, regional distending forces are reflected by pleural pressure ($P_{\rm PL}$). Thus, vertical gradients of $P_{\rm PL}$ (Krueger et al., 1961) and regional lung volume are a direct consequence of static gravitational stress distributions within the lung.

If the lung is considered as a large number of gas exchange units each exhibiting a characteristic pressure-volume (P-V) relationship similar to the whole lung, the influence of pleural pressure gradients on regional ventilation is illustrated in Figure 1. Ventilation will depend on both the resting P_{PL} and the change in P_{PL} (Δ P_{PL}). By virtue of the gravity dependent gradients of $P_{\rm pL}$ and regional volume, lung regions will operate at different points along the P-V curve. If each unit is subjected to the same Δ $P_{\text{pl.}}$, optimum ventilation occurs when the lung acts as a single homogenous unit operating at the inflection point of the P-V curve (dV/dP = maximum). Regional inhomogeneities of ventilation develop when the lung deviates from this homogenous state. Ventilation is now determined by the distribution of units along the P-V curve, with ventilatory inhomogeneities dependent on both the width of the distribution and the mean operating point of the lung. At low lung volumes, apical lung regions may operate near the inflection point (ΔV_r) while basal areas are near their regional residual volume (RV_r) (Δ V $_{r_1}$). As overall lung volume is increased, each unit moves along the P-V curve with apical regions approaching their regional total lung

Figure 1. A hypothetical regional pressure-volume (P-V) curve.

volume (RV $_{\Gamma}$) to regional total lung capacity (TLC $_{\Gamma}$) versus change in tidal volume (Δ V $_{r}$) for a given Δ P $_{TP}$ are illustrated for three lung Regional volume is plotted in arbitrary units from regional residual regions operating at different points along the P-V curve by virtue transpulmonary pressure ($\vartriangle~P_{\mathrm{TP}})$ in cm $\mathrm{H_2O}_{\mathrm{\bullet}}$. Regional variations in of the static vertical $\ensuremath{P_{\mathrm{TP}}}$ gradient.



capacity (TLC $_r$) (Δ V $_r$) and basal areas approaching their regional inflection point (Δ V $_r$) resulting in a progressive shift in the tidal volume toward the basal lung units.

This simple model can account for shifts in regional ventilation with lung volume (Milic-Emili et al., 1966) on the basis of static gravitational stresses, but the actual change in $\boldsymbol{P}_{\text{PL}}$ seen by a given region is dependent on the interaction of the lung and chest wall, and may not be constant for all regions. Pleural surface pressure has been measured in rabbits and dogs without the introduction of a cannula into the pleural space by placing a clear, rigid capsule over an exposed area of the parietal pleura and adjusting capsule pressure to remove any visible deformations in the local lung surface (Agostoni et al., The distribution of pleural pressure is dependent on body position, the gradient of transdiaphragmatic pressure and chest wall conformation (Agostoni et al., 1970; Agostoni and D'Angelo, 1971). In particular, diaphragmatic position and visceral contents exert a major effect on pleural surface pressures, with evisceration resulting in a 2-3 fold reduction in the vertical $P_{\rm pl.}$ gradient. In laterally recumbent man, voluntary diaphragmatic contraction reduces the vertical differences in 133 Xe concentrations, reflecting a more uniform distribution of regional volumes and ventilation (Roussos et al., 1977). This shift in the regional volume distribution may be the result of a change in diaphragmatic conformation and the gradient of P_{PI} during voluntary diaphragmatic contraction. Rehder et al. (1977) used the same technique to assess changes in regional ventilatory inhomogeneities following

anesthesia and paralysis in man. In lateral recumbency, anesthetizedparalyzed mechanically ventilated subjects show greater regional differences in ¹³³Xe concentration than awake spontaneously breathing man.
Thus, changes in chest wall shape and alterations in the transmission
of forces between the lung and chest wall appear to be major factors
influencing the regional distribution of ventilation.

While lung and chest wall interactions determine intrapleural pressure, lung expansion is dependent on the transmission of $P_{\rm PL}$ through the lung parenchyma. Mead et al. (1970) modelled lung expansion as a sum of all distending and recoil stresses acting on a lung unit. When the lung is expanded homogeneously, net distending force on interdependent airspaces depends directly on pleural pressure. When interdependent regions do not expand uniformly, the effective distending pressures acting on the regions reflect the degree of mechanical interdependence and no longer bear a direct relation to $P_{\rm PL}$. Mechanical interdependence acts to reduce local inhomogeneities of ventilation by changing the stress distributions between interdependent regions. The distribution of ventilation within the lung is then a function of static gravitational stresses, the transmission of forces from the thoracic and diaphragmatic surfaces through the lung parenchyma, and local stress distributions between mechanically interdependent structures.

The uptake or clearance of an inert gas by ventilation has also been used to assess distributions of lung volume. If the lung is assumed to be a single well mixed compartment of volume V and tidal volume $V_{\rm T}$ (Figure 2A), the expired concentration of an inert gas such as

N₂ distributed in the lung obeys the following difference equation when the inspired indicator concentration is zero:

$$F_{N_{L}}(n+1) = F_{N_{2}}(n) \left[\frac{V}{V+V_{T}}\right]$$
 (1)

where:

$$n$$
 = breath number $F_{N_2}(n)$ = fractional expired N_2 concentration at breath n

Equation 1 may be written in terms of a dimensionless N_2 concentration (F'_{N_2}) , and in general form is given by (Appendix):

$$\mathbf{F'}_{N_2}$$
 (n) = $\frac{\mathbf{F}_{N_2}$ (n) - \mathbf{F}_{N_2} (\infty) (\infty) = $\left[\frac{\mathbf{V}}{\mathbf{V} + \mathbf{V}_{\mathbf{T}}}\right]^n$ (2)

where:

$$F_{N_2}^{(n)}$$
 (n) = dimensionless N_2 concentration at breath n $F_{N_2}^{(0)}$, $F_{N_2}^{(n)}$, $F_{N_2}^{(\infty)}$ = fractional N_2 concentration at breath 0, n, and ∞ respectively.

Deviations of expired N_2 concentration from the relationship given by equation 2 may be, in part, accounted for by the presence of more than one compartment. The model can be extended to k parallel, independent compartments (k = 2, Figure 2B) by the addition of a weighting factor to account for differences in compartmental tidal volumes (V_{T_1}), and assuming all k compartments start at the same initial condition (F_{N_2} (0)), can be shown to follow:

Figure 2. Four compartmental representations of the lung.

- A) Single compartment, no deadspace.
- B) Two compartment, no deadspace.
- C) Single compartment with deadspace.
- D) Two compartment, common deadspace.

Compartments are assumed to be instantaneously mixed, with the volume and tidal volume of the compartment represented by V and V_T respectively. Deadspace volume (V_D) is assumed to have a flat velocity profile and undergo no diffusive mixing with the compartments.

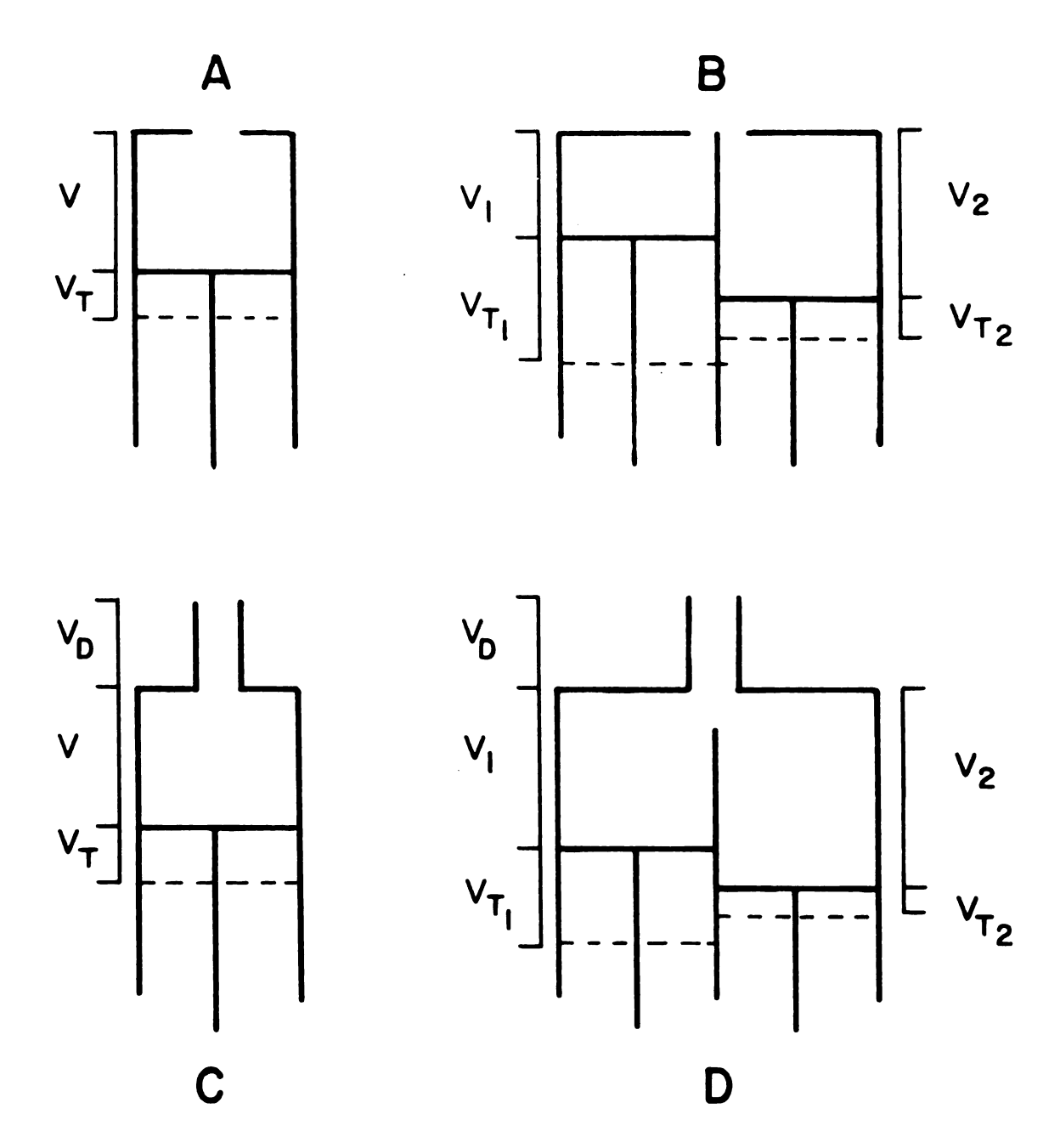


Figure 2

$$F'_{N_2}(n) = \frac{1}{V_T} \sum_{i=1}^k V_{T_i} \begin{bmatrix} V_i \\ V_i + V_{T_i} \end{bmatrix}^n$$
(3)

where:

$$V_{T} = \sum_{i=1}^{k} V_{T_{i}}$$

This model separates the lung into functionally different compartments based on their clearance rates. The number of unique compartments that can be resolved is limited by the method of analysis. Numerical solutions have been used to resolve up to four compartments and analog simulation has been used to define as many as six independent compartments (Fowler et al., 1952; Hashimoto et al., 1967).

One major criticism of these models is the failure to incorporate a deadspace volume (V_D). The addition of deadspace to the model of Figure 2A is shown in Figure 2C. Again, the compartment is assumed to be instantaneously well mixed. In addition, flow within V_D is assumed to have a flat velocity profile (plug flow) with no diffusive mixing occurring between V_D and V. Because of the initial expiration of deadspace gas at the inspired N_D concentration, $F_{N_D}^{\dagger}$ (n) is now based on an 'end-tidal' sample and is given by:

$$F'_{N_2}(n) = \left[\frac{V+V_D}{V+V_T}\right]^n$$
 (4)

This equation was presented by Darling et al. (1944). The extension to k parallel compartments with independent deadspaces is similar to the previous case (Appendix). This multiple compartment model reveals a significant amount of uneven ventilation in normal man, and an increase

in these ventilatory inhomogeneities with obstructive pulmonary disease (Fowler et al., 1952; Hashimoto et al., 1967; Tsunodo et al., 1972).

An alternative to assuming an independent deadspace associated with each compartment is the addition of a common deadspace to a two compartment system (Figure 2D) as developed by Weber and Bouhuys (1959)

(Appendix):
$$F'_{N_{2}}(n) = \begin{pmatrix} v_{T_{1}} & v_{T_{2}} \\ \hline v_{T} & v_{T_{2}} \end{pmatrix} \begin{pmatrix} v_{0} & m_{0} \\ v_{0} & q_{0} \end{pmatrix}^{n} \begin{pmatrix} 1 \\ 1 \end{pmatrix}$$
where:
$$k_{0} = \frac{v_{1} + \begin{pmatrix} v_{T_{1}} \\ \hline v_{T} \end{pmatrix} v_{D}}{v_{1} + v_{T_{1}}}$$

$$m_{0} = \frac{\begin{pmatrix} v_{T_{1}} \\ \hline v_{T} \end{pmatrix} \begin{pmatrix} v_{T_{2}} \\ \hline v_{T} \end{pmatrix} v_{D}}{v_{1} + v_{T_{1}}}$$

$$q_{0} = \frac{v_{2} + \begin{pmatrix} v_{T_{2}} \\ \hline v_{T} \end{pmatrix} v_{D}}{v_{2} + v_{T_{2}}}$$

$$q_{0} = \frac{v_{2} + \begin{pmatrix} v_{T_{2}} \\ \hline v_{T} \end{pmatrix} v_{D}}{v_{2} + v_{T_{2}}}$$

In the presence of a common mixing chamber (V_D) , clearance of the inert gas from the two compartments are interdependent, and clearance rates for the individual compartments are no longer exponential; better ventilated unit clearances being relatively retarded and poorly ventilated unit clearances enhanced. As a result, indicator clearance, as measured by mixed end-expired concentration at the mouth, appears more uniform with increasing V_D .

In contrast to approximating the lung as a small finite number of compartments, two major approaches have been proposed to model the lung as a continuous distribution of some characteristic defining the

indicator clearance. The k compartment model (equation 3) is extended to an integral equation by allowing k to approach infinity and compartment size to approach zero. Nakamura et al. (1966) and Okubo and Lenfant (1968) have modelled the lung washout function as a continuous distribution of clearance time constants. This technique makes the initial assumption that indicator washout is continuous in time. All models for indicator clearance assume that the parameters governing the washout are constant. In the case of the difference equations 1-5, one primary constraint is on the constancy of tidal volume (V_T) . When the washout is defined as a function in time rather than breath number, both depth $(V_{_{\mathbf{T}}})$ and respiratory rate must be constant. The spontaneously ventilating anesthetized horse exhibits greater variations in respiratory rate than V_{π} during the washout maneuvers, making analysis in time subject to large errors. The equations of Gomez (1963) take into account the discontinuous nature of ventilation by modelling the lung as a distribution of specific tidal volume (V $_{\!_{\boldsymbol{T}}}/V$, ξ). Gomez and Filler (1966) proposed approximating the expired indicator concentration during an open circuit washout with the equation:

$$F'_{N_2}(n) = \frac{1}{(1+an)^2}$$
 (6)

where:

a,z = empirical constants
n = breath number

By solving for the parameters a and z with a generalized non-linear least squares algorithm (Bevington, 1969) and evaluating the inverse Laplace transform of equation 6, a continuous distribution in terms of

relative number of units as a function of ξ is obtained (Appendix). Characteristics of the distribution (mean, mode, half-width) have been used to determine changes in the distribution of ventilation in both normal man and patients with pulmonary pathologies (Gomez et al., 1964; Filler and Gomez, 1966). There have been no studies where open circuit multiple breath indicator dilutions have been used to determine ventilatory inhomogeneities during anesthesia.

The lung models described above have been primarily concerned with inhomogeneities of lung volume and tidal volume, and do not account for regional differences in emptying rates; i.e., sequential or asynchronous ventilation. Fowler (1949) investigated uneven ventilation using a single breath of 100% 0_2 and noted three phases in expired F_{N_2} : 1) deadspace gas (phase I), 2) a deadspace-alveolar boundary (phase II), and 3) an alveolar plateau (phase III). Asynchronous ventilation results in a non-zero slope of the alveolar plateau, and depends on regional differences in both indicator concentration and emptying rates (Fowler, 1949). Milic-Emili et al. (1966), measuring regional inhomogeneities of 133Xe distributions, demonstrated that upper lung units are relatively better ventilated than lower units near RV, with the opposite case found near TLC. As a result, boli of 133 Xe inhaled at RV are preferentially distributed to upper lung regions during a vital capacity (VC) inspiration (Anthonisen et al., 1970). The pattern of lung emptying from TLC is reversed from the direction of filling, and a positive slope of the alveolar plateau is seen as non-dependent, indicator rich regions make progressively greater contributions to the expirate. By rotating

both standing and laterally recumbent subjects 180° after receiving a bolus of 133 Xe during a VC inspiration, the vertical distribution of indicator is inverted relative to the gravitational field. The slope of phase III on the subsequent expiration is negative, and demonstrates that regional asynchronous lung emptying proceeds from the bottom to the top of the lung relative to the gravitational field, with the slope of the alveolar plateau dependent on the vertical distribution of the indicator at TLC (Anthonisen et al., 1970). Isolated dog lungs show similar behavior, with the regional distribution of 133 Xe dependent on the vertical gradient of transpulmonary pressure (Glaister et al., 1973B). In man, single breath N 2 washouts performed under zero gravity show little or no slope to the alveolar plateau (Michels and West, 1977), confirming that asynchronous ventilation is a result of the vertical distribution of gravitational stresses within the lung.

The single breath dilution experiment has also been used to evaluate small airway closure in dependent lung regions (Anthonisen et al., 1969). Following a VC inspriation of 100% O₂ from RV, regional N₂ concentration varies through the lung, with N₂ preferentially distributed to the upper lung regions. During the subsequent exhalation to RV, there may be a relatively abrupt change in the slope of the alveolar plateau, termed phase IV (Dollfuss et al., 1967), with the lung volume above RV at the onset of phase IV designated as closing volume (CV). From measurements of regional lung volume with inspired 133 Xe, dependent lung regions have been shown to reach their regional RV prior to the lung as a whole, indicating that basal lung units are either subject to

airway closure or their compliance approaches zero at low lung volumes (Milic-Emili et al., 1966).

If airway closure occurs, regions subjected to closure will trap gas and tend to develop atelectasis. The closed airway will also exhibit a critical opening pressure necessary to reopen the airway dependent on its radius and the surface tension of the airway fluid (Mead et al., 1957). By removing N_2 from any trapped gas, the development of absorption atelectasis is enhanced. Burger and Macklem (1968) measured increases in lung elastic recoil in human subjects following complete N_2 washout with 100% O_2 and tidal breathing at RV or breath holding at RV, and revealed a significant amount of airway closure below 20% VC. When the lung volume is equilibrated with an inspired indicator, indicator concentration at equilibrium is dependent on the volume of thoracic gas communicating with the mouth. Any gas trapped behind closed airways will not equilibrate with the indicator. If the lung is now inflated to a high lung volume such that the closed airways open, the sequestered trapped gas will cause a proportionate decrease in indicator concentration. Using this method, small airway closure has been demonstrated in both conscious and anesthetized man (Burger and Macklem, 1968; Don et al., 1972). If N₂O is distributed throughout the lung, Engel et al. (1975) observed that a 133 Xe bolus at the mouth will be drawn into the lungs as N₂O is absorbed during a breath hold with an open glottis, and the 133 Xe will be distributed according to regional blood flow provided the airways are patent. Regional 133Xe concentrations following a bolus of 133 Xe inhaled or given intravenously provide

indices of regional ventilation and perfusion respectively. At low lung volumes, dependent lung regions were found to receive less inhaled 133 Xe than predicted on the basis of their regional blood flow. This was attributed to the presence of airway closure preventing the replacement of absorbed N₂O with 133 Xe (Engel et al., 1975).

While airway closure is a sufficient condition to account for the presence of phase IV during the single breath N, washout, the only requirement for phase IV to occur is a change in regional contributions to the expirate. The lung operates within a pressure-flow-volume relationship bounded by a maximal flow-volume curve. At any given lung volume, expiratory flow is limited by dynamic airway compression and becomes independent of effort (Fry et al., 1958). Since dependent lung regions reach their regional RV first (Milic-Emili et al., 1966), for a given expiratory flow rate, dependent lung units may begin operating on their maximal flow-volume curve prior to the remainder of the lung, and make progressively smaller contributions to the total expirate due to flow limitation. Regional flow limitation was advanced by Hyatt et al. (1973) and Rodarte et al. (1975) to explain the flow dependence of CV in man. In contrast to man, the onset of phase IV is relatively flow independent in the dog (Lai et al., 1977), and the contribution of this mechanism to the development of phase IV may be species specific. However, the presence of phase IV during a single breath N_2 washout, either by virtue of small airway closure or regional flow limitation, does reflect an impairment of ventilation in dependent lung regions.

Regional inhomogeneities of ventilation have been demonstrated in both conscious and anesthetized man. These include regional differences in volumes and tidal volumes, and asynchronous ventilation between lung regions. The distribution of ventilation is dependent on gravitational stress distributions, lung-chest wall interactions, and local stress distributions between mechanically interdependent lung units. Uneven ventilation has been implicated as a factor influencing gas exchange during anesthesia. In particular, airway closure has been cited as a major cause of impaired arterial oxygenation in anesthetized man. Further, a significant portion of the changes in gas exchange with anesthesia in man are related to postural changes. Since the mechanisms influencing gas exchange during general anesthesia may be similar for man and horse, inhomogeneities of ventilation were investigated using multiple and single breath N₂ dilution tests, and the distribution of ventilation determined as a function of body position.

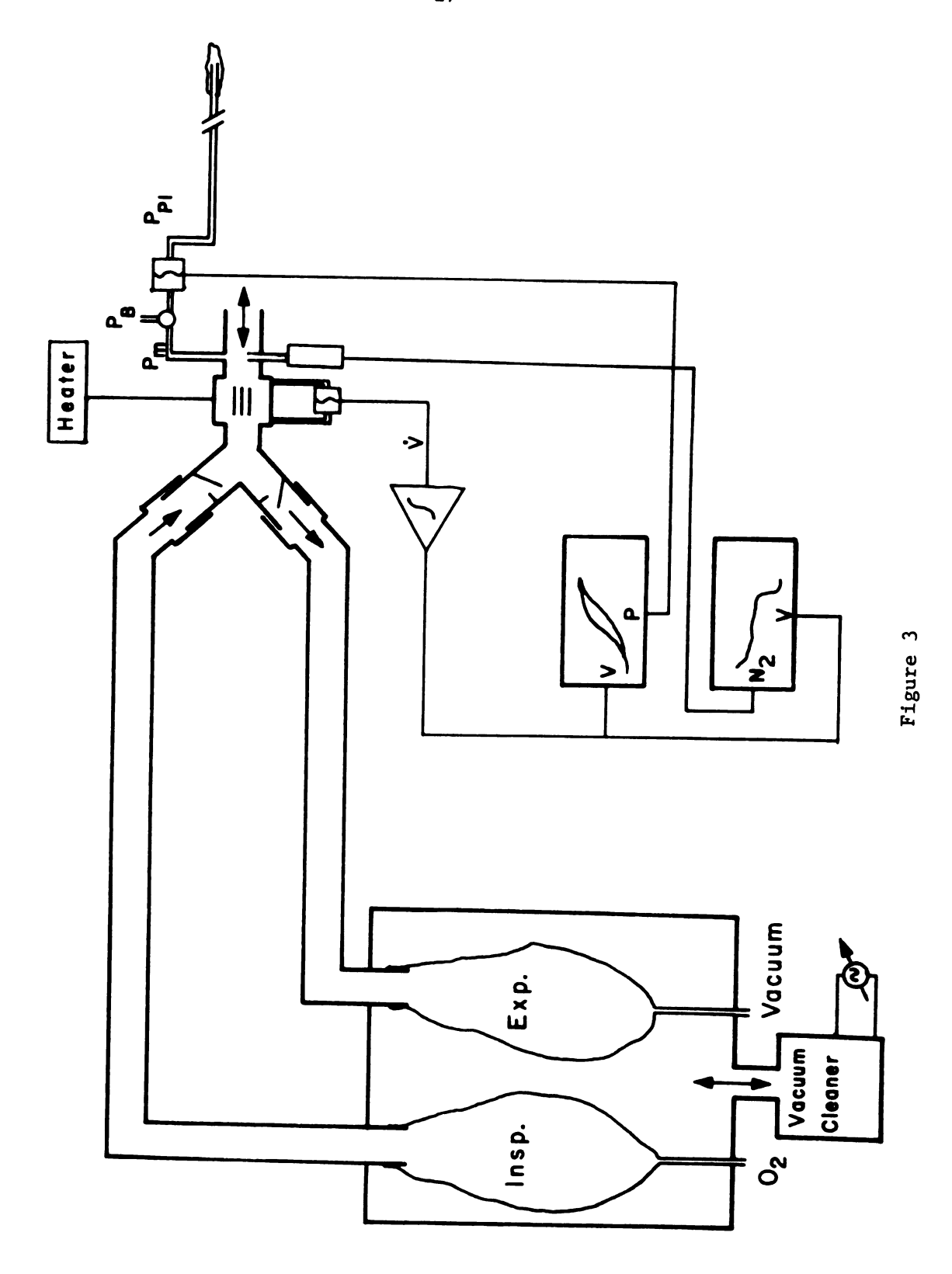
MATERIALS AND METHODS

Pressure-volume Experiments

Eight horses weighing 395-541 kg (\overline{X} = 485 kg) were restrained, and a stomach tube with a 10 cm long esophageal balloon (Anode Rubber Plating Co., Boling, Texas) attached to its outer wall was passed into the esophagus via the nares. The balloon was positioned in the midthorax by visually approximating the distance from the nares to the 10th intercostal space. Animals were subsequently anesthetized (2% glycerol guaiacolate and 0.2% sodium thiamylal, i.v.) and placed into lateral recumbency. The trachea was intubated and anesthesia was maintained by a continuous infusion of the anesthetic solution with depth adjusted to maintain a palpebral reflex.

For measurement of esophageal pressure, the lumen of the stomach tube was sealed and the volume of the esophageal balloon adjusted to 0.5 ml. Esophageal pressure was monitored and the balloon repositioned, if necessary, to give good dynamic response and a negative excursion on inspiration. Changes in pleural pressure (P_{PL}), as reflected by esophageal pressure, were measured with a differential pressure transducer (PM131, Statham Instruments, Hato Rey, Puerto Rico) calibrated against a water manometer. Transpulmonary (P_{TP}) and transthoracic (P_{TT}) pressure were recorded by measuring P_{PL} with respect to either mouth (P_{M}) or atmospheric (P_{R}) pressure (Figure 3).

recording of quasi-static pressure-volume curves and single breath N_2 washouts. and plotted against transpulmonary pressure ($^{
m P}_{
m P}$ $^{
m -P}_{
m DL}$) or transthoracic pressure measured with a heated pneumotachograph-pressure transducer-integrator system Inspiration and expiration were controlled with a variable transformer-vacuum cleaner attached to a dual bag in box system. Inspired (100% $^{0}_{2}$) and expired Schematic representation of the experimental equipment used for simultaneous gas were separated by one way valves at the mouth. Ventilatory volumes were $(P_{\rm PL}-P_{\rm B})$ and $N_{\rm 2}$ concentration on two X-Y recorders. Figure 3.



Nitrogen concentration (F_{N2}) was monitored at the mouth with a rapidly responding N₂ analyzer (Cardio-pulmonary Instrument Corporation, Houston, Texas) having a specified linearity of 1% full scale and calibrated to an electronic 0% N₂ derived within the analyzer and 79% N₂ using room air. Inspired and expired volumes were measured by electronic integration of the flow signal generated by a pneumotachograph (Fleisch #4, Dynasciences, Blue Bell, Pennsylvania) and differential pressure transducer (PM5, Statham Instruments). The pneumotachograph was heated to prevent vapor condensation and the pneumotachograph-transducer—integrator system was calibrated using known flows (1-6 1/sec) delivered via a rotameter (Fischer and Porter Co., Warminster, Pennsylvania).

Quasi-static pressure-volume (P-V) curves of the lung and thorax were recorded while simultaneously performing a single breath N_2 washout. Horses were studied in left lateral, right lateral, dorsal, and sternal recumbency with the sequence of positions randomized by a latin square design. At the end of a normal expiration (functional residual capacity, FRC), the endotracheal tube was attached to a dual 100 l bag in box system (Figure 3) with one-way valves for separation of inspired and expired gases. A vacuum cleaner controlled by a variable transformer was used to deflate the lungs to a $P_{\rm TP}$ less than -30 cm H_2O (defined as residual volume, RV), slowly inflate the lungs with 100% O_2 to a $P_{\rm TP}$ greater than 30 cm H_2O (defined as total lung capacity, TLC), and slowly return the lungs to RV. The complete maneuver was performed in 60-90 secs. X-Y recorders (Hewlett-Packard Co., Palo Alto, California) were used to plot volume versus pressure and N_2 concentration

versus volume. Five maneuvers were performed in each position, three monitoring P_{TP} and two monitoring P_{TT} . A sample record is shown in Figure 4 with volume measured relative to RV, and P_{TP} and P_{TT} measured relative to resting levels (P_{M} = 0 cm H_{2} 0). Expiratory reserve volume (ER) was measured as the volume expired from FRC to RV, and chest wall compliance (C_{CW}) was calculated from the slope of the recordings of volume versus P_{TT} over a tidal volume (5 1) started at FRC (Figure 4).

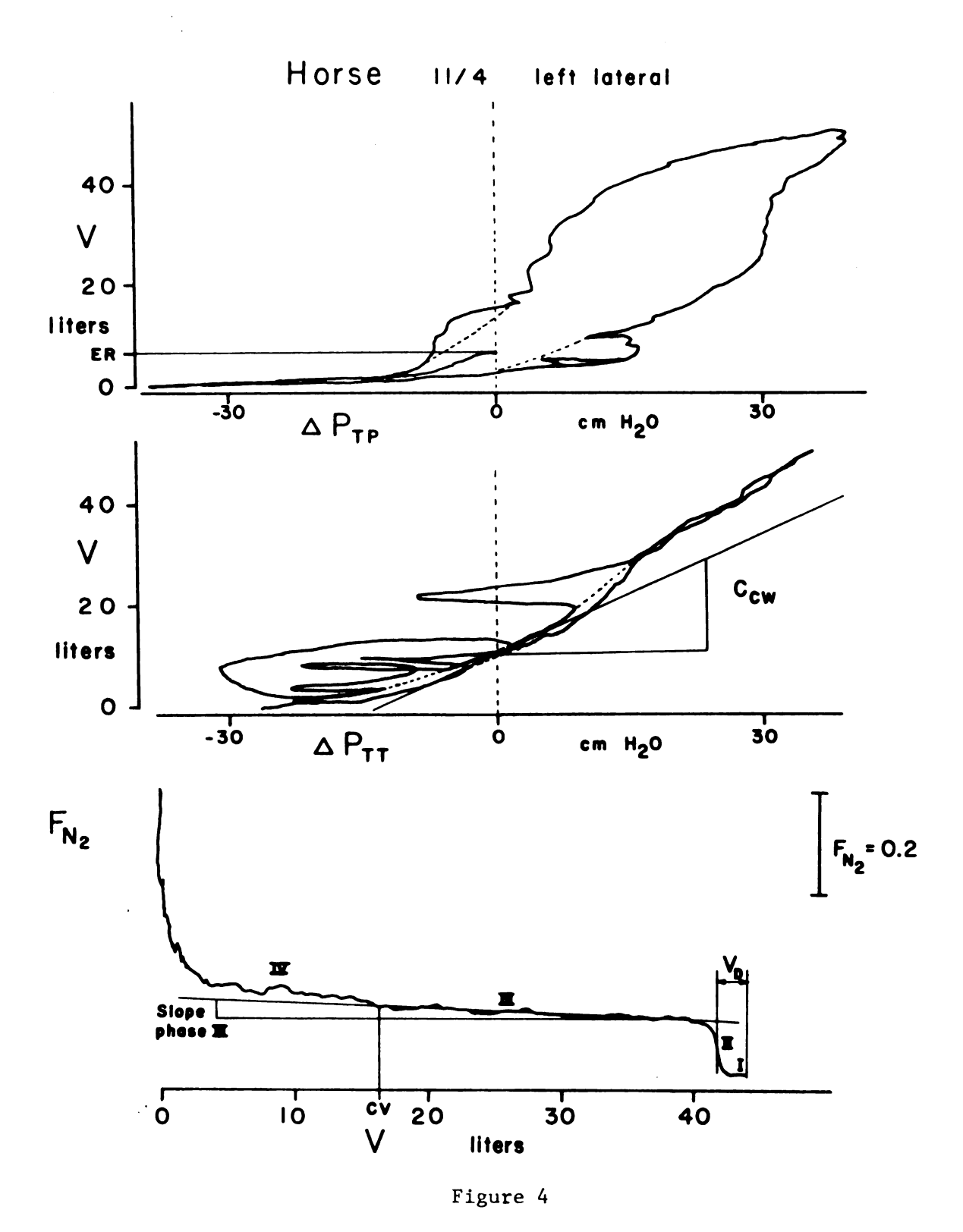
Due to differences in P_{TP} at end inflation both between animals and between successive maneuvers, a standardized treatment of the lung P-V curve was adopted. Fifty to one hundred coordinates of lung volume measured relative to RV and distending pressure measured relative to resting P_{TP} were taken from the expiratory limb of three lung P-V curves and fitted to a general sigmoid function proposed by Murphy and Engel (1977):

$$P = \frac{k_1}{V_{MAX} - V} + \frac{k_2}{V_{MIN} - V} + k_3$$
 (7)

 V_{MAX} and V_{MIN} represent the two volume asymptotes (TLC and RV respectively) with k_1 , k_2 , and k_3 defining the shape of the curve. Since volume was measured with respect to RV (V_{MIN}) , the equation of Murphy and Engel was rewritten with V_{MIN} set to zero to express volume as a function of pressure:

$$V = \frac{-b - \sqrt{b^2 - 4ac}}{2a} \tag{8}$$

Figure 4. Representative recordings of quasi-static lung (P_{TP}) and thoracic (P_{TT}) P-V curves and the single breath N_2 washout. Pressure-volume curves are plotted as volume in liters above RV (V = 0 1) versus change in distending pressure (ΔP_{TP} or ΔP_{TT}) in cm H_2^0 from the resting level ($P_M = 0$ cm H_2^0). Expiratory reserve volume (ER) was taken as the volume exhaled from FRC ($P_M = 0$ cm H_2^0) to RV (V = 0 1). Chest wall compliance (C_{CW}) was taken as the slope of the chest wall P-V curve over a tidal volume (5 1) started at FRC. Respiratory efforts appear as large pressure excursions away from the visually smoothed P-V curve (dotted line). Single breath N_2 washout is plotted as fractional N_2 concentration (F_{N_2}) versus lung volume in liters above RV (V = 0 1). Phases I-IV, anatomic deadspace (V_D), closing volume (CV), and slope of the alveolar plateau (phase III) are designated.



where:

$$a = k_3 - P$$

 $b = V_{MAX}(P-k_3) - k_1 - k_2$
 $c = V_{MAX}(k_2)^3$

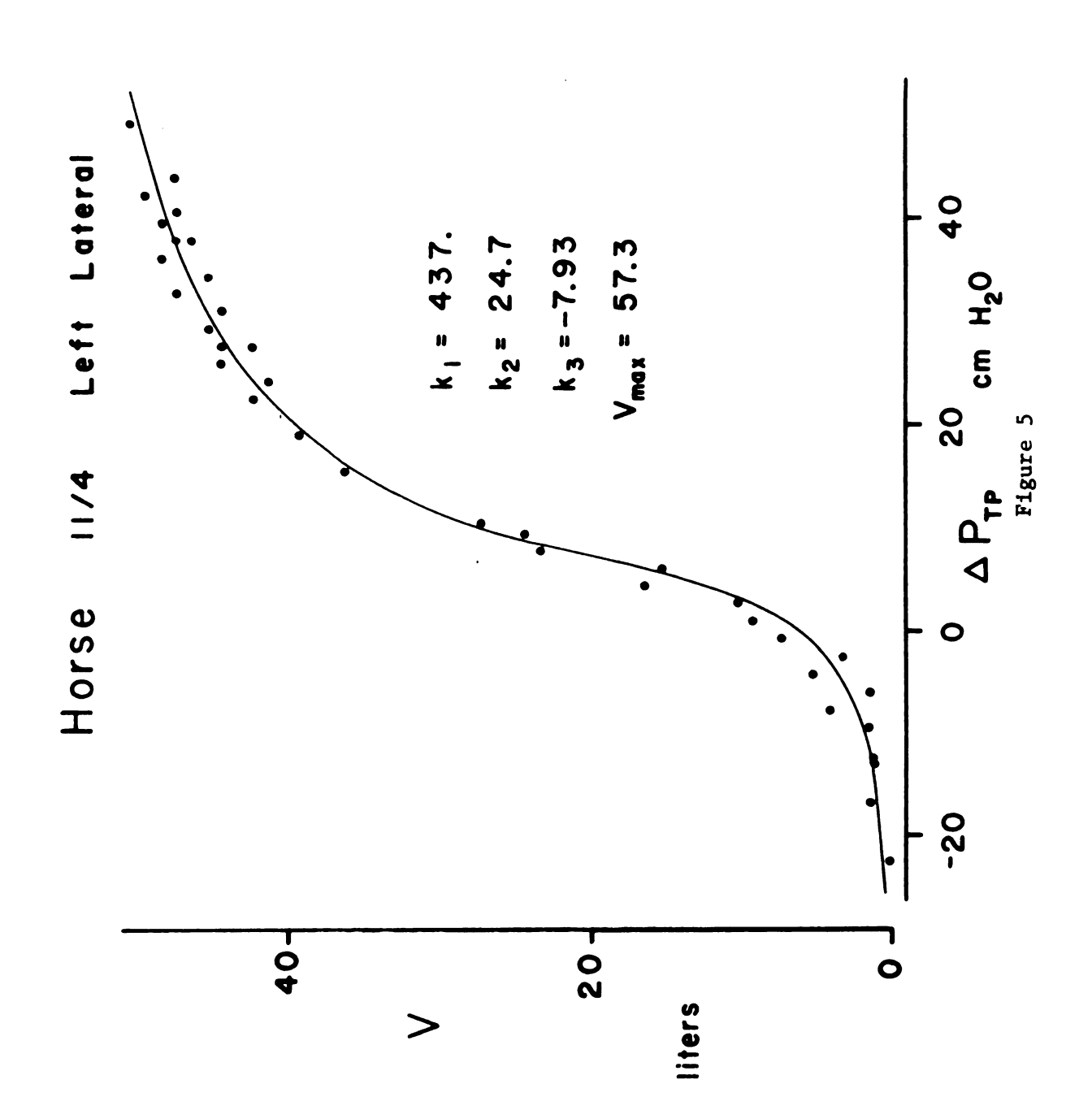
the parameters of equation 8 were determined by minimizing the residuals (measured V - predicted V) with a non-linear least squares algorithm (Bevington, 1969) performed by a digital computer (LSI-11, Digital Equipment Corporation, Maynard, Massachusetts) (Figure 5). FORTRAN source programs for the fitting algorithm are given in Bevington (1969). The maximum lung volume (V_{MAX}), vital capacity (VC) defined as the predicted volume at a distending pressure of 30 cm H_2O , the coordinates of the inflection point ($d^2V/dP^2 = O$, P_{IP} , V_{IP}), and lung compliance (C_L) defined as the slope of the function over a tidal volume (5 1) started at $P_M = O$ cm H_2O were determined from the parameters of equation 8 in each body position.

Expired N_2 concentration is subdivided into four phases (Figure 4): phase I represents anatomic deadspace, phase II is the deadspace—alveolar boundary, phase III is an alveolar plateau, and phase IV represents a departure in F_{N_2} from the earlier portion of the plateau. Five F_{N_2} versus volume records taken during the P-V maneuvers were analyzed to determine anatomic deadspace (V_D), the slope of the alveolar plateau, and the onset of phase IV (closing volume, CV) (Figure 4). Deadspace was estimated by bisecting phase II with respect to N_2 concentration. The slope of phase III was determined by drawing the best straight line through the initial portion of the plateau. Closing volume was then determined as the first point at which F_{N_2} made a permanent departure

Results of non-linear least squares fit of equation 8. Figure 5.

curves plotted as lung volume in liters above $RV \ (V = 0 \ l)$ versus change $(P_{\rm M}=0~{\rm cm}~{\rm H_2}0)$ of a horse in left lateral recumbency. The smooth curve Fifty-six points were taken from the expiratory limb of three lung P-V was generated from the four parameters of equation 8 given in the in transpulmonary pressure $(\Delta P_{\mathrm{TP}},~\text{cm}~H_2^{\,0})$ from the resting level

figure.



from the alveolar plateau. The distending pressure at CV (P_{CV}) was determined using the estimated parameters of equation 8.

The influence of position on the P-V characteristics of the lung and the parameters of the single breath $\rm N_2$ washout were analyzed by a two-way analysis of variance (ANOVA) with differences between body positions evaluated with Student-Newman-Keuls (SNK) procedure (Sokal and Rohlf, 1969).

Closed Circuit N_2 Experiments

Closed circuit N_2 equilibrations were performed on 8 anesthetized horses with an average weight of 488 kg (range = 380-540 kg). Anesthesia was induced as previously described and equilibrations performed in left lateral, right lateral, dorsal, and sternal recumbency (sequence randomized). The closed circuit N_2 equilibrations were performed with a 120 l spirometer- CO_2 absorbant circle system (Figure 6). A known volume of 100% O_2 was added to the spirometer (V_0) such that the system contains a known quantity of N_2 contained in a known volume (V_1). At the end of a normal expiration, the lungs contain a known concentration of V_1 (V_1) in an unknown volume (functional residual capacity, FRC). By connecting the horse to the closed circuit spirometer system at end expiration, and maintaining spirometer volume constant by the addition of 100% V_2 , the equilibrium V_2 concentration in the lungs and spirometer may be used to determine FRC:

$$FRC = \frac{F_{N_2}(\infty) V_{O_2}}{F_{N_2}(0) - F_{N_2}(\infty)} - V_S$$
 (9)

Figure 6. Schematic diagram of equipment used to perform closed circuit N_2 equilibrations. The horse was attached to a 120 1 spirometer via one-way valves and expired through a CO_2 absorbant. Spirometer volume and N_2 concentration at the mouth were recorded continuously on a strip chart recorder.

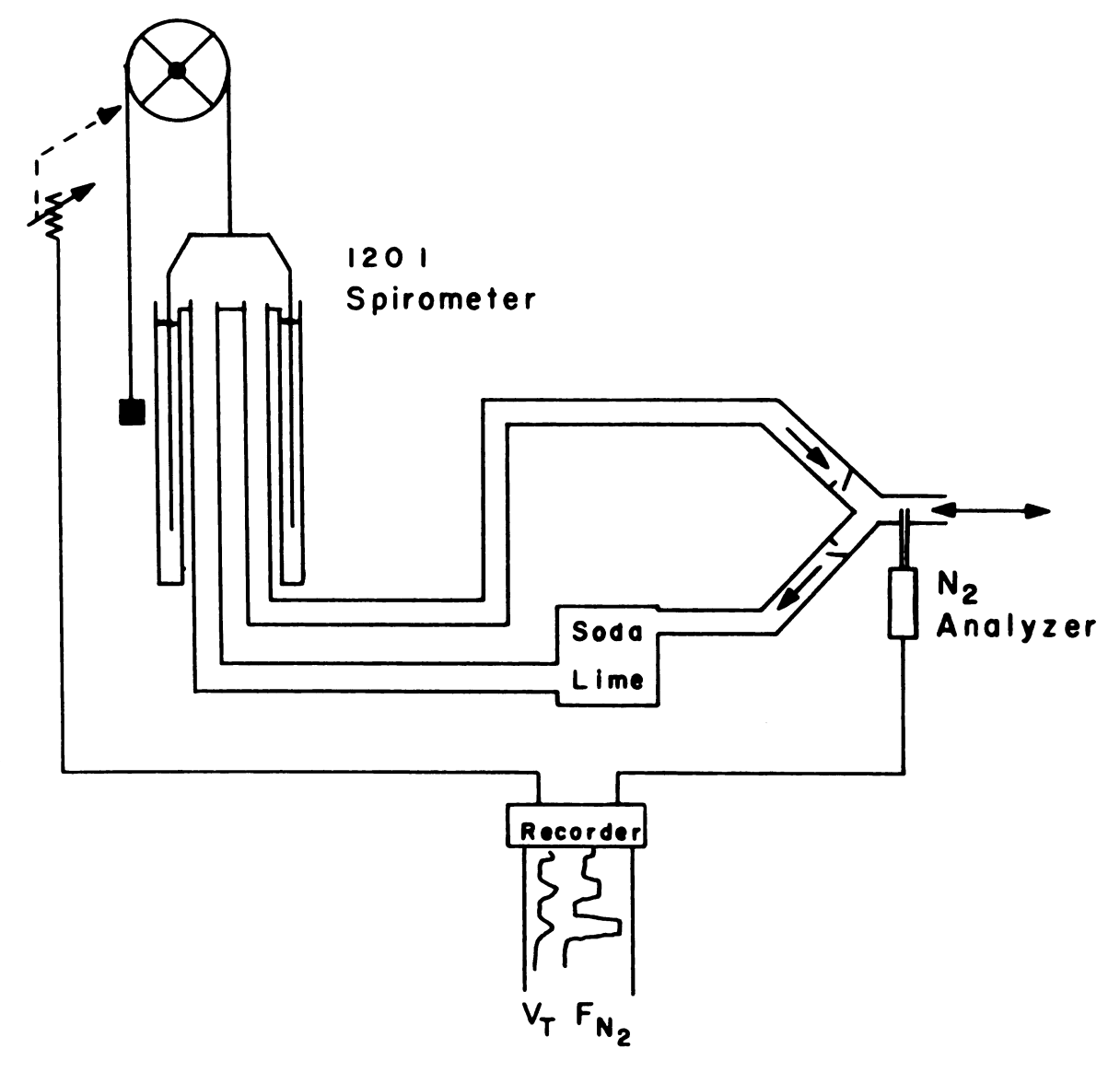


Figure 6

where:

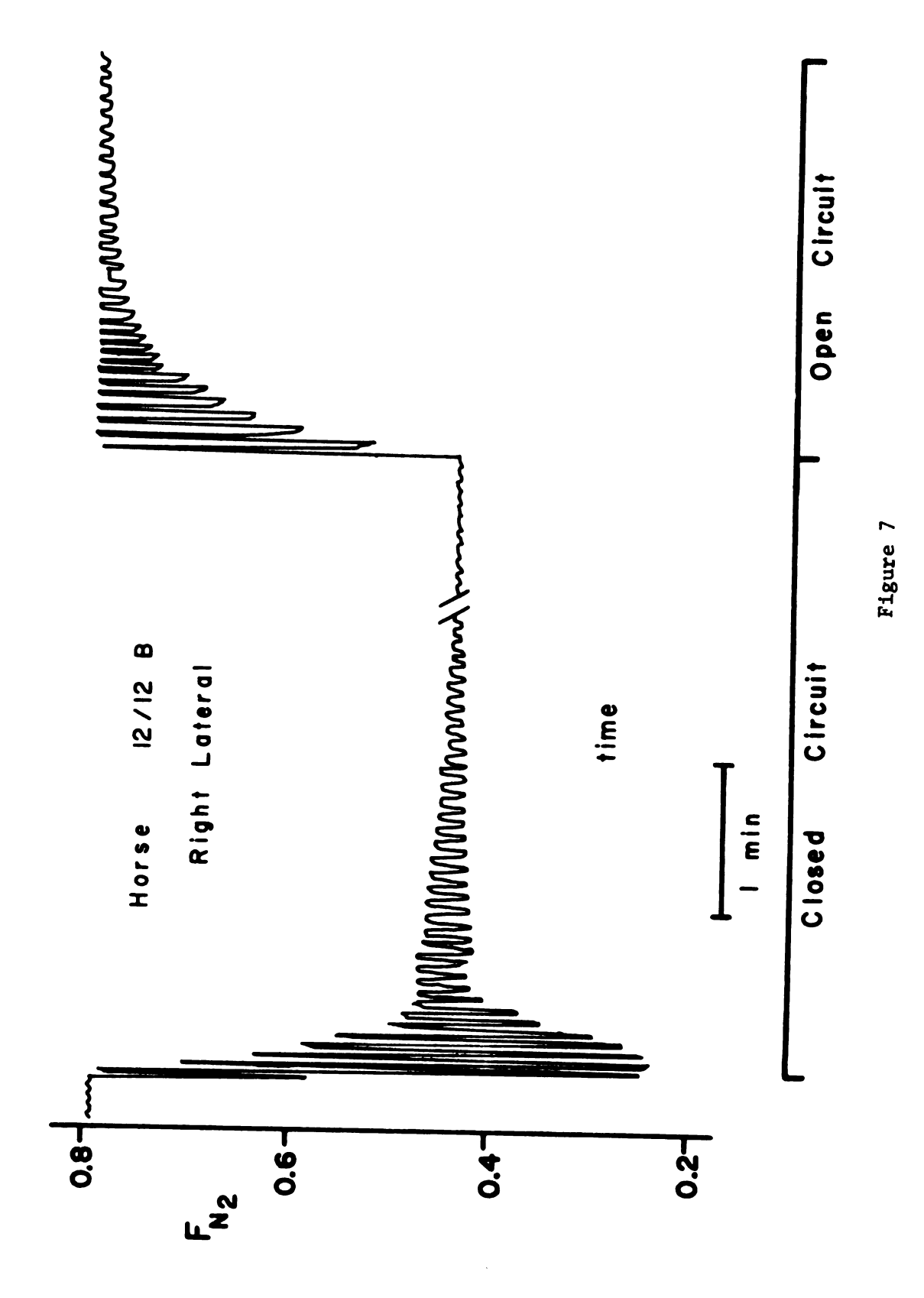
 $F_{N_2}(0)$ = initial N_2 concentration of system $F_{N_2}(\infty)$ = equilibrium N_2 concentration $V_{0_2}(\infty)$ = initial volume of 100% $V_{0_2}(\infty)$ added to spirometer $V_{0_2}(\infty)$ = volume of system deadspaces

System deadspace was substantial due to the large diameter tubing (approximately 6 cm) and large CO, absorbant canister necessary to reduce the resistance to breathing. The volume of the system deadspace was independently measured by replacing the animal with an empty 10 1 rebreathing bag ('FRC' = 0 1) and performing the closed circuit equilibration ($V_S \pm SE = 36.10 \pm 0.26 \, 1$, n = 6). Following equilibration, the inspiratory line was disconnected from the one-way valve at the end of a normal expiration and the washin of ${\rm N}_2$ monitored. The spirometer system was subsequently reconnected to the expiratory one-way valve to record expired tidal volume during the washin. A sample record showing the ${\rm N_2}$ equilibration followed by the ${\rm N_2}$ washin is shown in Figure 7. Expired N_2 concentration at breath n was expressed as a dimensionless N_2 concentration (F $^{\dagger}_{N_2}$, equation 2, Appendix) and analyzed using the models for 1) two compartment, no deadspace (2 Comp), 2) two compartment with equal, parallel deadspace (2 $Comp + V_D$), 3) two compartment, common deadspace (Weber-Bouhuys) (Weber and Bouhuys, 1959), and 4) the continuous distribution of specific tidal volume (Gomez) (Gomez, 1963). The influence of position on FRC and the model results was determined using a two-way ANOVA and SNK procedure.

Figure 7. Representative recording of fractional N_2 concentration versus time

during a closed circuit N_{2} equilibration and subsequent open circuit

N₂ washin.



RESULTS

Pressure-volume characteristics of the horse's respiratory system were determined from quasi-static pressure-volume (P-V) curves of the lung and thorax (Figure 4). In the initial experiments, attempts were made to induce apnea prior to recording a P-V curve. However, it was impossible to entrain the horses to a respirator, and the maneuvers had to be performed in the presence of occasional respiratory efforts. Respiratory movements produced the largest artifacts on the P-V curves of the thorax, shown as large pressure 'loops' away from a smooth P-V relationship (Figure 4). Cardiogenic artifacts were also superimposed on the P-V curve. To standardize interanimal treatment of the data, the expiratory limb of the lung P-V curve was first visually smoothed and coordinates of the P-V curve were then subjected to a non-linear least squares fit to equation 8 (Methods). The results of the curve fit to experimental data are shown in Figure 5. The predictive capability of equation 8 was good, with a mean residual (measured V-predicted V) of 0.1 liters and average variance of 2.7 1 for all body positions in all horses. Composite expiratory P-V curves were computed for each body position and are shown in Figure 8.

Several parameters of the quasi-static P-V curves are reported in Table 1. The estimated maximum lung volume (V_{MAX}) calculated from equation 8 was not altered by body position. Vital capacity (VC),

against the change in transpulmonary pressure $(\Delta P_{\rm TP})$ in cm $\rm H_2^{\, O}$ from resting Figure 8. Composite expiratory quasi-static lung P-V curves determined from 8 horses in four body positions. Volume in liters above RV (V = $0\ 1$) is plotted $P_{TP} (P_M = 0 \text{ cm } H_2^0)$.

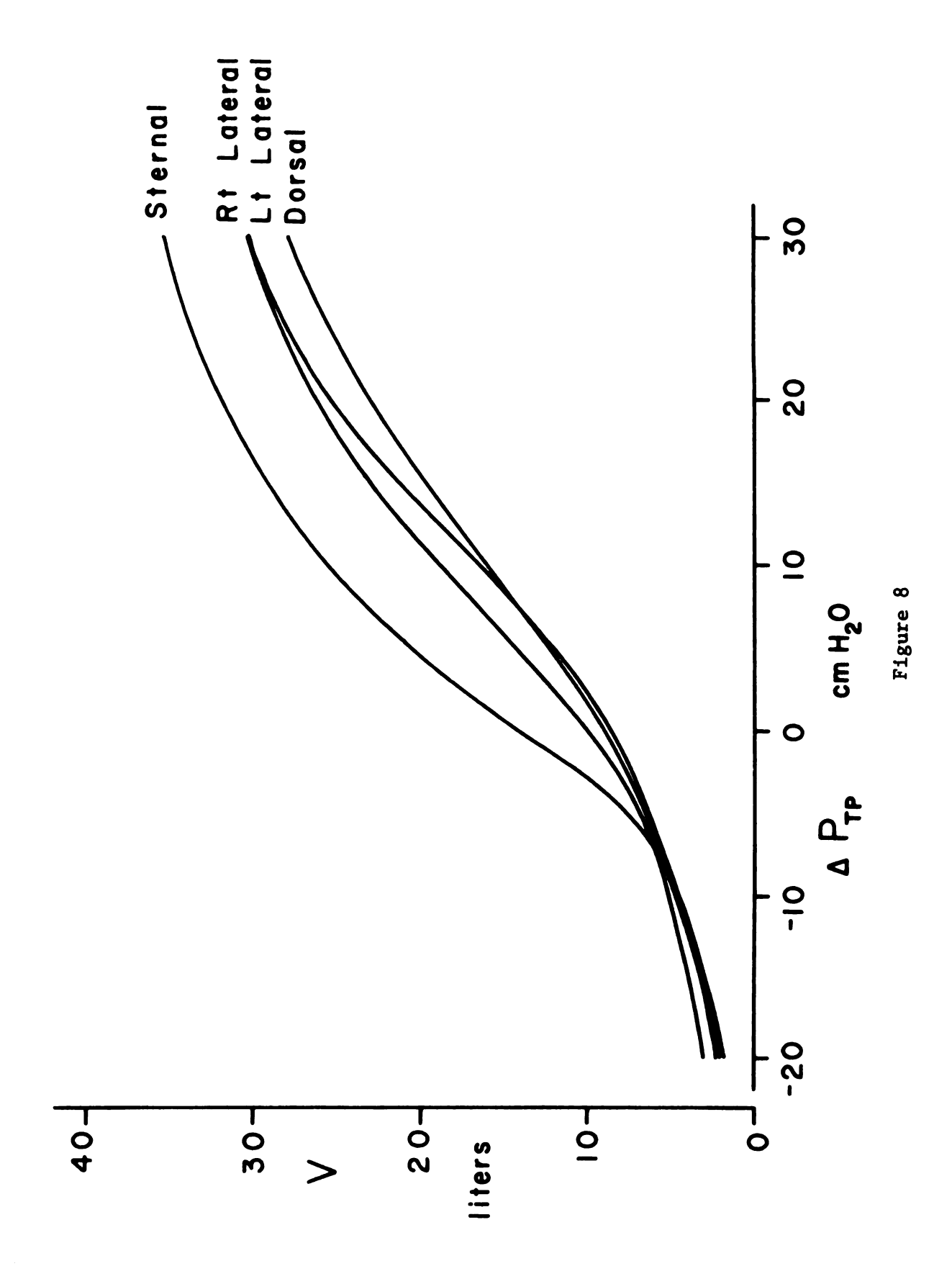


Table 1. Lung volumes (liters) determined from quasi-static P-V curves of the lung as a function of body position.

	Position					
	lt lat	rt lat	dorsal	sternal	SE	
V _{MAX}	42.	44.	59.	48.	6.9	
VC	30.	31.	28.*	36.	2.4	
ER	6.*	5.*	6.*	8.	0.5	

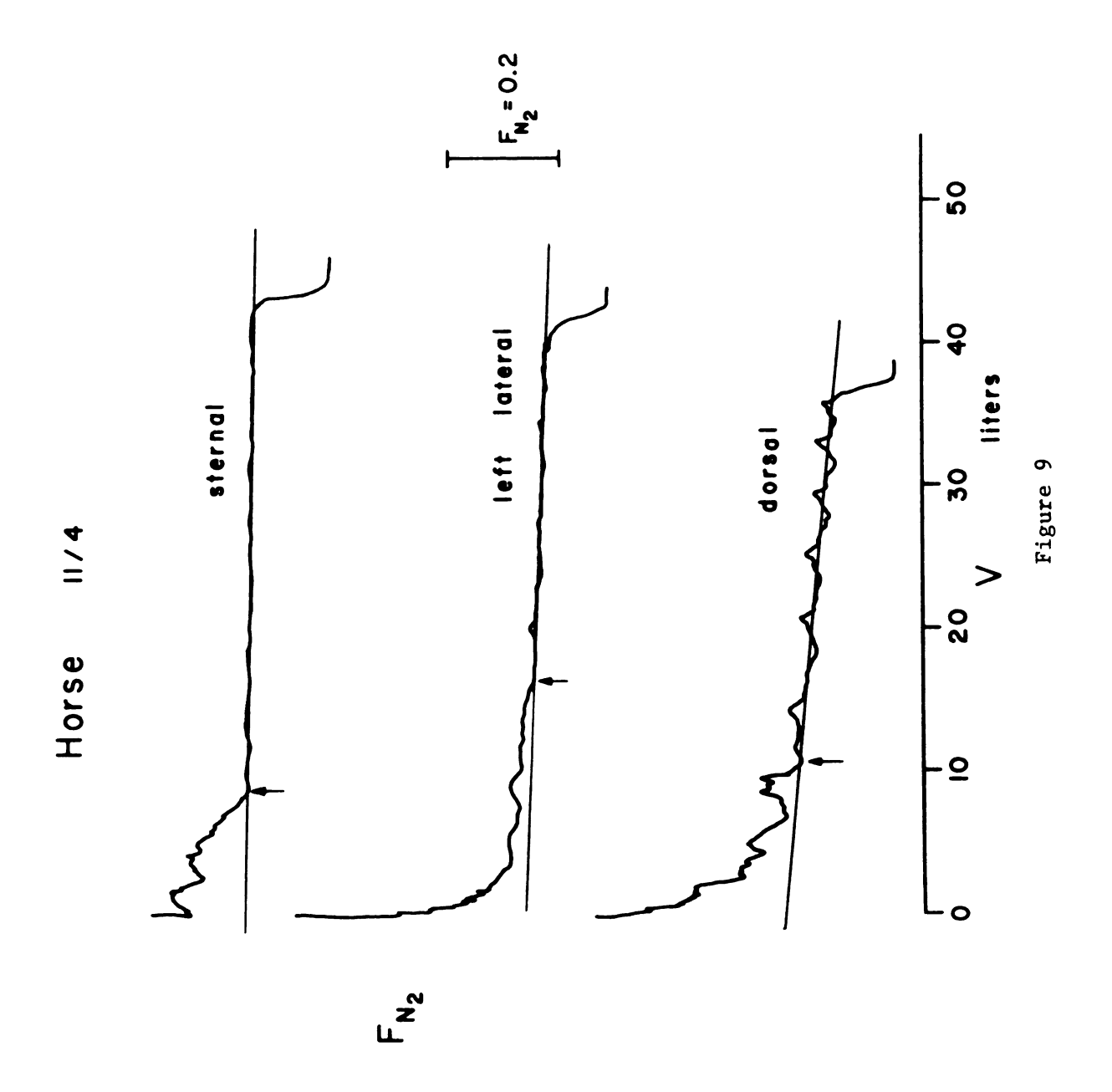
^{*}Significantly different (P < 0.05) from values obtained in sternal recumbency

SE = standard error of mean based on error mean square from ANOVA n = 8

defined as the lung volume above residual volume (RV) at a distending pressure of 30 cm $\rm H_2^{0}$, and expiratory reserve volume (ER) were significantly increased in sternal recumbency over the lateral and dorsal postures. Due to large interanimal variations, there were no significant changes in lung ($\rm C_L$) or chest wall ($\rm C_{CW}$) compliance with posture, averaging 1.3 \pm 0.1 and 0.6 \pm 0.1 1/cm $\rm H_2^{0}$ 0 respectively ($\rm \overline{X}$ \pm SE, n = 8). Values similar to these for $\rm C_L$ and $\rm C_{CW}$ have been reported in both awake, standing, and anesthetized, suspended upright horses (Gillespie et al., 1966; Leith and Gillespie, 1971).

The effect of position on the single breath N₂ washout in one animal is shown in Figure 9. Parameters defined by the single breath N₂ washout were analyzed as a function of posture. Anatomic deadspace (V_D) did not vary with body position, and averaged 2.1 \pm 0.1 1 (\overline{X} \pm SE, n = 8). There was a significant decrease in the slope of the alveolar

of phase IV, defined as the first permanent departure of \boldsymbol{F}_{N_2} from the alveolar Effect of position on the single breath ${\rm N_2}$ washout for one horse. Expired ${\rm N_2}$ plateau to determine the slope of the plateau. The arrow indicates the onset volume in liters (RV = 0 1). A straight line was drawn through the alveolar concentration was recorded as fractional ${\rm N_2}$ concentration ${\rm (F_N)}$ versus lung plateau. Figure 9.



plateau (phase III) in sternal versus lateral and dorsal recumbency (Table 2). The onset of phase IV (closing volume, CV) in liters above RV and the distending pressure at CV (P_{CV}) calculated from the parameters of equation 8 (Methods) did not change with posture (Table 2). Closing volume (Table 2) was significantly greater than ER (Table 1) in the lateral and dorsal postures.

Table 2. Values for parameters of the single breath ${\rm N}_2$ washout test in different body positions.

	lt lat	rt lat	dorsal	sternal	SE
Slope of phase III (F _{N2} .10 ² .1)	0.30*	0.36*	0.35*	0.13	0.03
CV (1)	9.	9.	9.	9.	0.8
P _{CV} (cm H ₂ O)	1.2	-1.9	0.8	-4.2	1.44
V _{IP} (1)	12.	12.	12.	14.	0.8
P _{IP} (cm H ₂ O)	4.6	2.8	4.0	0.1	1.57

^{*}Significant difference (P < 0.05) from sternal recumbency SE = standard error of mean based on error mean square from ANOVA n = 8

Previous investigations have suggested a strong correlation between the distending pressure and lung volume at the onset of phase IV (P_{CV} , CV) and the P-V coordinates at the inflection point of the lung P-V curve (P_{IP} , V_{IP}) (Ingram et al., 1974; Glaister et al., 1973B). The coordinates of the inflection point (P_{IP} , V_{IP}) did not vary with

body position (Table 2). Correlation coefficients (r) were computed between P_{CV} and P_{IP} , and CV and V_{IP} and significance determined from a table of critical values for r (P<0.05) (Rohlf and Sokal, 1969). Significant correlations between CV and V_{IP} were seen in all but sternal recumbency, while a correlation between P_{CV} and P_{IP} was seen only in left lateral and sternal recumbency. If the data is combined without respect to body position, the correlations of CV on V_{IP} (r = 0.76, n = 32) and P_{CV} on P_{IP} (r = 0.78, n = 32) were significant.

Mean values for functional residual capacity (FRC) in the various postures determined from the closed circuit N_2 equilibration are shown in Table 3, and compared with an estimated FRC based on the open circuit N_2 washin as predicted by five models of the lung. One animal's results were excluded from the closed circuit equilibration results due to a leak in the spirometer system, and one animal's results were excluded from the open circuit washin results due to a very erratic breathing pattern in dorsal recumbency. Tidal volume (V_T) did not vary with body position $(\overline{X} = 6.41, SE = 0.51)$, and FRC was significantly increased in sternal recumbency over the other postures (Table 3).

To assess the influence of position on the distribution of ventilation, data from the open circuit N_2 washins were subjected to a nonlinear least squares curve fitting algorithm to obtain solutions to three basic equations. For a two compartment lung with no deadspace (2 Comp), the dimensionless N_2 concentration (F' N_2) at breath n given by equation 3 (k = 2, Appendix) may be rewritten as:

$$F_{N_2}^{(n)} = (A)(B)^n + (1-A)(C)^n$$
 (10)

Table 3. Estimated functional residual capacity (FRC, liters) given by closed and open circuit ${\rm N}_2$ dilution experiments.

Position	Closed Circuit	2 Comp + V _D	Weber- Bouhuys	Open † Circuit Gomez + V D	2 Comp	Gomez
lt lat	12.1	11.3	11.7	12.5	18.6*	20.0*
rt lat	11.8	14.4	14.5	16.2	21.8*	23.7*
dorsal	12.0	15.8	14.5	16.5	22.6*	25.0*
sternal	24.7	25.4	25.5	30.7 [‡]	38.2 [‡]	45.8*
SE	1.5	2.1	2.4	3.3	3.5	4.8

^{*}Significantly different (P < 0.05) from closed circuit, 2 Comp + $\rm V_D$, Weber-Bouhuys, and Gomez + $\rm V_D$ models

2 compartment model with no deadspace 2 Comp:

2 Comp + V_D : 2 compartment model with equal, parallel deadspace

Weber-Bouhuys: 2 compartment model with common deadspace

Gomez: continuous distribution of specific tidal volume Gomez + V_D :

Gomez model based on the effective specific tidal volume $(V'_T = V_T - V_D)$

^{*}Significantly different from all other positions

SE = standard error of mean based on error mean square from ANOVA n = 6 †Models for lung clearance are designated in Tables 3-6 as:

where:

$$A = v_{T_{1}}/v_{T}$$

$$B = v_{1}/(v_{1} + v_{T_{1}})$$

$$C = v_{2}/(v_{2} + v_{T} - v_{T_{1}})$$

and:

$$v_{T_2} = v_{T} - v_{T_1}$$

Using the mean V_T measured during the washin, the estimated parameters, A, B, and C, may be used to estimate FRC $(V_1 + V_2)$ (2 Comp, Table 3). The same parameters, A, B, and C, may also be applied to a two compartment model assuming parallel, equal deadspaces (k = 2, equation 20, Appendix). The parameters of equation 10 are now redefined as:

$$A = V_{T_{1}}/V_{T}$$

$$B = (V_{1} + V_{D}/2)/(V_{1} + V_{T_{1}})$$

$$C = (V_{2} + V_{D}/2)/(V_{2} + V_{T} - V_{T_{1}})$$

The mean value for V_D obtained from the single breath N_2 washout (2.1 1) was taken as the best estimate of V_D , and the average V_T during the washin calculated. Given V_T and V_D , V_1 , V_2 , V_{T_1} , V_{T_2} , and an estimate of FRC ($V_1 + V_2 + V_D$) may be determined from the parameters of equation 10. The model (2 Comp + V_D) estimates for the compartment volumes and tidal volume are given in Table 5, and estimated FRC is given in Table 3.

The model of Weber and Bouhuys (equation 6, Appendix) was found to converge on experimental data erratically when the minimization algorithm manipulated either the volumes and tidal volumes of the compartments directly or the parameters k_0 , m_0 , p_0 , and q_0 . A possible reason for this failure to converge on a solution is that the parameters of equation 6 were not constant during the washin. However, this constraint is also imposed on the other lung models and indicates that variability in the parameters may not be responsible for the erratic behavior of the fitting algorithm. Since V_T must be considered to be constant throughout the washin and V_D can be estimated from the value determined by the single breath N_2 washout, the model can be reduced to only three unknowns: V_{T_1} , V_1 , and V_2 . It should then be possible to define the Weber-Bouhuys model with only three parameters which may be easier to solve for than the original parameters k_0 - q_0 . By dividing k_0 by m_0 and q_0 by p_0 , three new parameters were defined:

$$A = V_{T_1}/V_{T}$$

$$B = \frac{V_1 + \left(\frac{V_{T_1}}{V_T}\right)^2 V_D}{\left(\frac{V_{T_1}}{V_T}\right)^2 \left(\frac{V_{T_2}}{V_T}\right)^2 V_D}$$

$$C = \frac{V_2 + \left(\frac{V_{T_2}}{V_T}\right)^2 V_D}{\left(\frac{V_{T_2}}{V_T}\right)^2 V_D}$$

The curve fitting algorithm was able to manipulate A, B, and C, and converge reliably on a solution. Again, given V_T and V_D , A, B, and C may be solved for the compartment volumes, tidal volumes, and FRC (Weber-Bouhuys, Tables 3 and 5).

Finally, the parameters a and z of equation 7 (Appendix) were manipulated directly and the distribution of specific tidal volume defined by equation 28 (Appendix) computed. The mean value of this distribution ($\overline{\xi}$) corresponds to V_T/FRC . Thus, knowing V_T , FRC may be calculated (Gomez, Table 3). This model does not explicitly account for deadspace, but by using an effective tidal volume ($V_T = V_T - V_D$) in place of V_T , a second estimate of FRC based on $\overline{\xi}$ is obtained (Gomez + V_D , Table 3).

The results of applying these models to an experimental washin is shown in Figure 10. Visually there was no difference between the functions used to approximate the washin. To evaluate which model best describes the behavior of the lung, the variance of the residuals of F'N were compared with an F ratio test (Sokel and Rohlf, 1969). Mean values for the residual variance from the solutions of the three basic equations used to define the N2 washin were not significantly different (Table 4) indicating that all the models predict the washin function equally well. Models extended to three and four compartments never resulted in a better approximation of the dilution phenomena. Also, single compartment models never gave a satisfactory fit to the data.

Dimensionless N_2 concentration $(F^{\tau}_{N_3})$ plotted against breath number (n) predicted $\mathbf{F^t}_N$ given by non-linear least squares fitting to the models parallel V_{D} (k = 2, equation 20), and with common V_{D} (equation 5), and for a horse in right lateral recumbency. Smooth curve represents the 2) the continuous distribution of specific tidal volume (equation 6). for: 1) two compartment without V_D (k = 2, equation 3), with equal Figure 10.

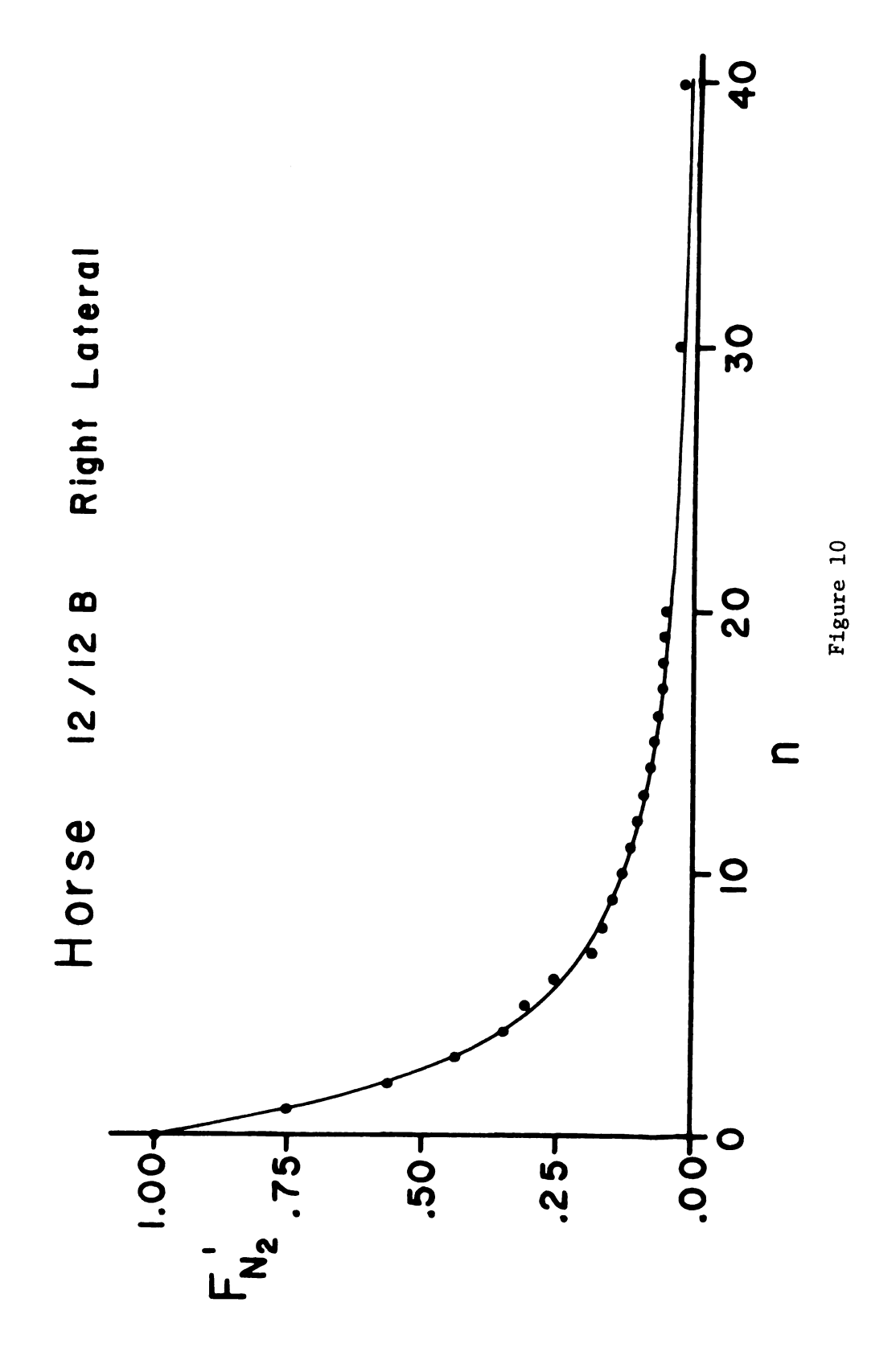


Table 4. Variance of residuals (measured F_{N_2} - predicted F_{N_2}) X 10^4 for the three basic lung models investigated.

Model [†] Position 2 Comp Weber-Bouhuys Gomez							
lt lat	1.19	1.18	1.44				
rt lat	1.97	1.96	2.32				
dorsal	2.94	2.85	4.27				
sternal	1.10	1.10	1.28				

Model designations as given in Table 3.

Comparisons between the model estimates of FRC and FRC determined by closed circuit N_2 equilibration are given in Table 3. In all cases, FRC was significantly elevated in sternal recumbency. The importance of considering deadspace in modelling the open circuit N_2 dilution function is illustrated by the agreement in estimated FRC with a standard method for determination of FRC (closed circuit equilibration) even though a common value of V_D was assumed for all animals. Without the inclusion of a deadspace volume (2 Comp, Gomez) FRC was significantly greater than the estimates obtained from the closed circuit N_2 equilibration and lung models incorporating V_D (2 Comp + V_D).

Because of the agreement between the closed circuit N_2 equilibration FRC and model estimates of FRC, the effect of position on individual compartment volumes and tidal volumes was only evaluated in the models incorporating V_D . The smaller volumed compartment (V_1) of the

Weber-Bouhuys model demonstrated a significant increase in volume and decrease in tidal volume (V_{T_1}) in sternal recumbency over the other postures. There was a significant increase in V_1 in sternal recumbency, but no change in V_{T_1} given by the two compartment parallel, equal deadspace model (2 Comp + V_D). The larger compartment (V_2) demonstrated no shift in tidal volume in either two compartment deadspace model, but had a larger estimated volume in dorsal and sternal recumbency than the lateral postures (Table 5).

The continuous distribution function of specific tidal volume (ξ) given by the model of Gomez (1963) (equation 28, Appendix) was highly variable and showed no consistent changes with posture. Mean values for a and z (equation 7, Appendix) were used to determine average distributions of ξ in three different body positions (Figure 11).

In assessing the distribution of ventilation, specific tidal volumes $(V_T/V, \xi)$ were compared using the effective tidal volume $(V_T' = V_T - V_D)$ for the three models incorporating V_D (Table 6). The fast compartment (largest ξ) was designated ξ_1 . In the parallel, equal deadspace two compartment model, V_{T_k}' is computed as $V_{T_k} - V_D/2$ for k = 1,2. In the Weber-Bouhuys model, V_{T_k}' is computed by weighting the relative contribution of V_D to each compartment $(V_T' = V_T - (V_T/V_T)(V_D), k = 1,2)$. A mean specific tidal volume (ξ) is given explicitly by the model of Gomez (equation 29, Appendix). There was no significant shift in estimated specific tidal volumes given by the Gomez or Weber-Bouhuys models with body position (Table 6). Specific tidal volume of the slow compartment was significantly elevated in left lateral

Table 5. Estimated compartment volumes and tidal volumes (liters) as a function of position given by the 2 compartment models[†] incorporating deadspace.

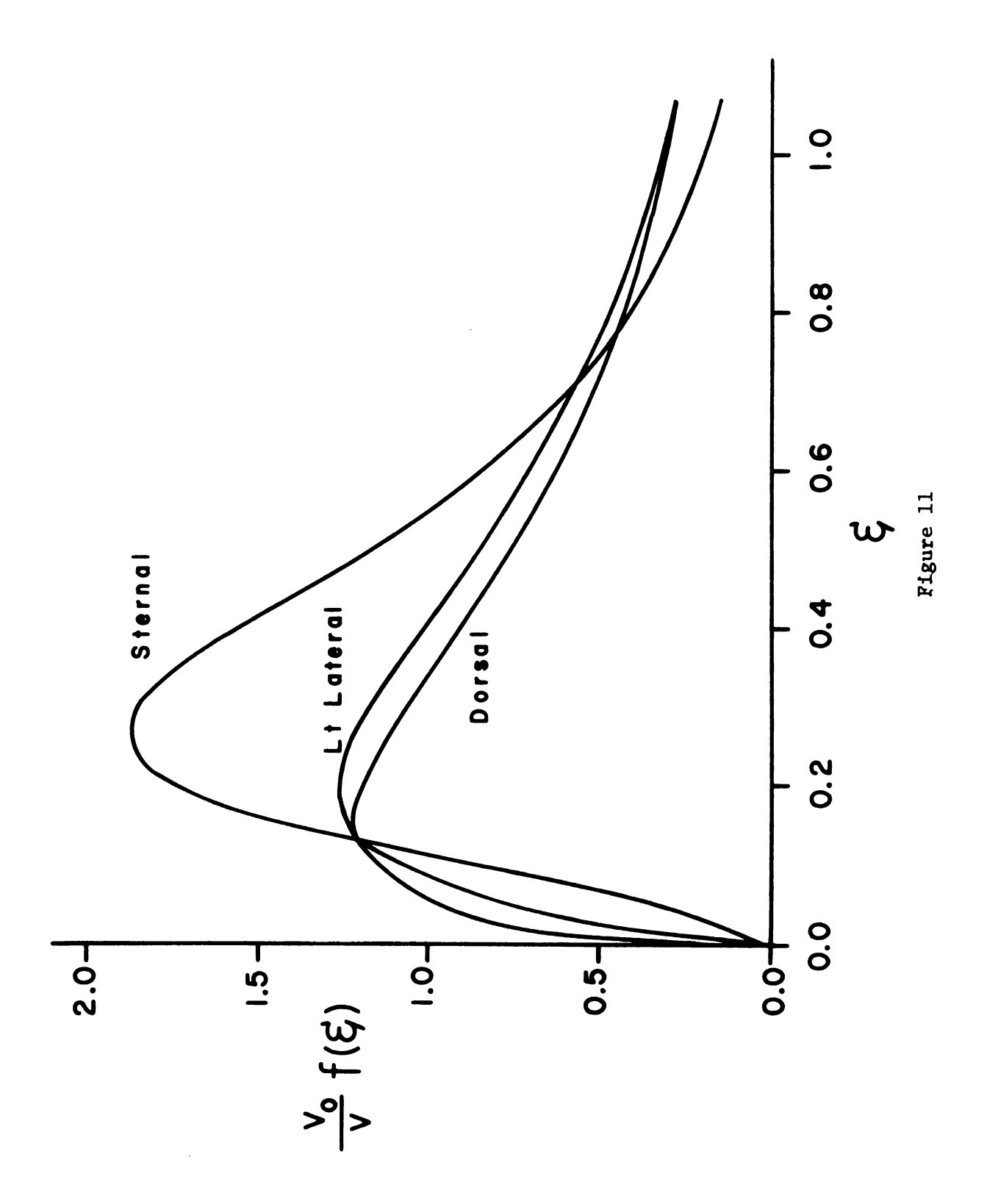
	Position					
	lt lat	rt lat	dorsal	sternal	SE	
v_{T_1}						
2 Comp + V _D	3.7	3.9	4.2	2.8	0.77	
Weber-Bouhuys	4.2	6.2*	4.6	3.4	0.67	
$v_{1}^{}$						
2 Comp + V _D	1.9*	4.0*	4.6*	5.2	0.79	
Weber-Bouhuys	2.6*	4.2*	3.8*	7.2	0.89	
v _{T2}						
2 Comp + V _D	2.7	3.0	2.0	3.3	0.55	
Weber-Bouhuys	2.2	0.6	1.6	3.0	0.58	
v						
V ₂ 2 Comp + V _D	7.0*	7.6*	11.5	17.1	0.69	
Weber-Bouhuys	6.5*	7.5*	11.2	15.4	2.09	

^{*}Significantly different (P < 0.05) from values obtained in sternal recumbency

SE = standard error of mean based on error mean square from ANOVA n = 7 † Model designations as given in Table 3

Figure 11. Mean distributions of specific tidal volume (ξ) given by the model of Notation is identical to that of Gomez (1963) with relative number of Gomez for 7 horses in three body positions (equation 28, Appendix).

units $(V_o/V \ f(\xi))$ plotted against specific tidal volume (ξ) .



recumbency for the two compartment parallel, equal deadspace model (2 Comp + V_n , Table 6).

Table 6. Specific tidal volume (ξ , V'_T/V) predicted from the model parameters using the effective tidal volume ($V'_T = V_T - V_D$) as a function of posture.

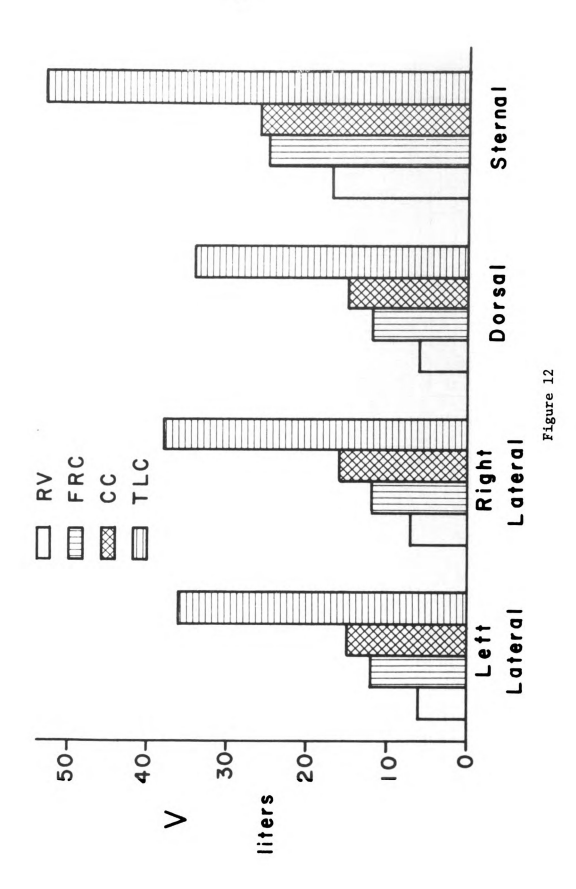
	Position				
Model [†]	lt lat	rt lat	dorsal	sternal	SE
2 Comp + V _D					
ξ ₁	1.73	1.45	0.82	0.58	0.35
ξ ₂	0.15*	0.09	0.06	0.07	0.02
Weber-Bouhuys					
ξ ₁	1.29	0.95	0.90	0.60	0.22
ξ ₂	0.10	0.06	0.05	0.06	0.02
Gomez + V _D					
ξ	0.38	0.31	0.27	0.23	0.06

Significant difference (P < 0.05) from all other postures SE = standard error of mean based on error mean square from ANOVA n = 7

By combining the results of the quasi-static P-V and single breath N₂ experiments with the closed circuit determination of FRC, sub-divisions of lung volume in the four positions may be estimated (Figure 12). Residual volume (RV) was obtained by subtracting ER (Table 1) from the closed circuit determination of FRC (Table 3).

 $^{^\}dagger$ Model designations as given in Table 3

volume (ER); closing capacity is the sum of closing volume (CV) and RV; body position. Residual volume (RV) was determined as the difference Figure 12. Estimated subdivisions of lung volume (V) in liters as a function of between functional residual capacity (FRC) and expiratory reserve total lung capacity is the sum of vital capacity (VC) and RV.



Total lung capacity (TLC) and closing capacity (CC) were calculated by adding RV to VC and CV respectively. In sternal recumbency, there was a large increase in RV and TLC from the lateral and dorsal postures, with FRC approaching CC.

DISCUSSION

These investigations have shown alterations in the distribution of lung volume and ventilation as a function of body position in the anesthetized horse. The major posturally related changes are a 50% reduction in functional residual capacity (FRC, Table 3), a three-fold increase in asynchronous ventilation (slope of phase III, Table 2), and a significant increase in closing volume (CV, Table 2) relative to expiratory reserve volume (ER, Table 1) as the animal moves from sternal into lateral or dorsal recumbency.

General anesthesia results in increased alveolar-arterial 0_2 tension differences (P_{A-a0}_2) , increased venous admixture (Q_S/Q_T) and a reduction in FRC in both man and horse (Nunn, 1969; Don et al., 1972; Hall et al., 1968; McDonell and Hall, 1974). In both conscious and anesthetized man, impaired gas exchange occurs when resting lung volume is less than the lung volume at which small airways are thought to close. Airway closure results in a lung region with ventilation-perfusion ratio (V/Q) of zero, contributing to venous admixture and hypoxemia. Positive airway pressures raise FRC in conscious and anesthetized subjects, and improve arterial oxygenation in patients whose FRC was reduced during anesthesia to 60% of the normal predicted value (Craig et al., 1972; Wyche et al., 1973). Improved gas exchange resulting from positive end-expiratory pressure has been attributed to

the increase in FRC. When FRC exceeds the lung volume at which airways \cdot · · · close, V/Q inequalities are reduced and arterial oxygenation aided.

In the present study, the relationship of resting lung volume to small airway closure in the anesthetized horse was assessed by simultaneously performing a quasi-static pressure-volume (P-V) maneuver and a modified single breath N_{2} washout. Following a vital capacity (VC) inspiration of 100% $\mathbf{0}_{2}$, regional \mathbf{N}_{2} concentration varies throughout the lung. This regional variation depends on differences in preinspiratory regional lung volume and on regional filling rates. During the subsequent expiration, expired N_2 concentration follows four characteristic phases (Figure 4); 1) phase I due to anatomic deadspace, 2) phase II, a deadspace-alveolar boundary, 3) phase III, an alveolar plateau, and 4) phase IV, any permanent deviation of N_2 concentration from phase III. The lung volume, in liters above residual volume (RV), at the onset of phase IV has been termed the closing volume of the lung (Dollfuss et al., 1967). Phase IV represents a significant alteration in the relative contribution of some lung region to the expirate. This change in relative regional emptying rate (phase IV) may be the result of: 1) small airway closure, 2) a regional compliance approaching zero, or 3) regional flow limitation.

The presence of small airway closure at low lung volumes has been well documented (Milic-Emili et al., 1966; Burger and Macklem, 1968; Engel et al., 1975). If a significant portion of the lung exhibits airway closure at some critical lung volume, those units undergoing closure cease to contribute to the expirate when lung volume falls below

the volume at which closure occurs. At this point, expired N_2 concentration makes an abrupt departure from the alveolar plateau. The onset of phase IV corresponds to the start of true airway closure.

When an airway closes, the region undergoing closure reaches its residual volume. Regional residual volume may also be determined by chest wall rigidity and local intrapulmonary stress distributions such that the effective regional compliance approaches zero (Leith and Mead, 1967; Mead et al., 1970). Again, the lung region involved ceases contributing to the expirate, resulting in the onset of phase IV. In this case, all airways remain patent.

The final mechanism advanced to explain phase IV of the single breath N₂ washout is regional flow limitation (Hyatt et al., 1973; Rodarte et al., 1975). As regional volume is reduced, regional flow may approach the local maximal expiratory flow. At this point, expiratory flow from the region becomes independent of expiratory effort and the relative contribution to the expirate from the flow limited segment is reduced, resulting in the onset of phase IV.

The relative contribution of each of these mechanisms to the onset of phase IV in this study is unknown. In addition, reporting a single critical lung volume at which 'closure' may occur (closing volume, CV, Table 2) should be interpreted with caution. If the lung were composed of two unique compartments, the onset of phase IV, by whatever mechanism, would appear as a sharp discontinuity in the alveolar plateau. As the lung deviates from behaving as two well-defined compartments, 'closure' takes on a more continuous nature throughout expiration, and smoothes

the onset of phase IV into a gradual transition between phases III and IV. Therefore, the onset of phase IV is best interpreted as that lung volume at which an appreciable portion of the lung undergoes some change in its relative pattern of emptying. In addition, despite the mechanism responsible, the presence of phase IV does represent a significant impairment of ventilation to some lung region when resting lung volume falls below CV. Since CV exceeds ER in all but sternal recumbency, a significant impairment of ventilation to dependent lung regions may exist during tidal breathing in the laterally and dorsally recumbent horse.

The contribution of regional flow limitation to phase IV was advanced to explain flow dependence of CV in man (Hyatt et al., 1973; Rodarte et al., 1975). These investigations found CV to vary with expiratory flow rates from 0.2 to 4.0 l/sec. However, Travis et al. (1973) did not find flow dependence of CV at respiratory flows below 1.4 l/sec in man, and Lai et al. (1977) reported a constant CV in the dog with flows up to 1.0 l/sec. In the present study, the single breath N₂ maneuver was performed in 60-90 secs, and required the movement of approximately 80 l of gas, giving a mean expiratory flow of 1-2 l/sec. At FRC, maximal expiratory flows in man and dog range from 6-8 l/sec (Macklem and Mead, 1968) as compared to 65-90 l/sec in the anesthetized upright horse (Leith and Gillespie, 1971). In sternal recumbency, CV was not significantly different from resting lung volume, indicating that the horse was operating at only 2/65 of its dynamic flow range (expiratory flow/maximal flow) at the onset of phase IV.

Flow independence of CV is seen in man and dog when the lung is deflating at less than 1/8 of its maximal expiratory flow. While regional flow limitation cannot be ruled out, by operating at lower fractions of the horse's dynamic flow range than those producing flow independence of CV in man and dog, the contribution of this mechanism to the development of phase IV in the horse is probably negligible.

While the contribution of true airway closure to the onset of phase IV is unknown, the quasi-static lung P-V curve provides more evidence as to the mechanism of phase IV in the horse. If an airway closes, a fluid meniscus forms in the closed airway. Both fluid surface tension in the meniscus and airway diameter determine a critical opening pressure necessary to recruit the closed segment. The loss of lung units due to airway closure also increases lung elastic recoil (Burger and Macklem, 1968). In the present study, lung compliance ($C_{\overline{L}}$) was not significantly altered by changes in position. However, there was an increase in VC and ER (Table 1) in sternal recumbency, and the mean lung P-V curves were shifted toward lower recoil pressure in the sternal posture. Furthermore, in many horses in dorsal and lateral recumbency, lung volume was still increasing with distending pressures in excess of $+45~\mathrm{cm}~\mathrm{H}_2^{~\mathrm{O}}$ when inflation was terminated. These findings support the contention that there were lung regions which were closed and exhibit high critical opening pressures. The empirical equation (equation 8) used to predict lung P-V behavior provides an estimate of maximal lung volume (V_{MAY}) . Maximal lung expansion is limited by tissue forces rather than surface tension forces, and the independence of $\boldsymbol{v}_{\text{MAX}}$ and

posture may reflect identical lung tissue properties and the potential for complete alveolar recruitment with higher inflation pressures.

From the single breath N_2 test, the onset of phase IV exceeded resting lung volume in all but sternal recumbency, indicating the presence of ventilatory inhomogeneities in dependent lung regions during tidal breathing in the lateral and dorsal postures. There was also an associated increase in lung elastic recoil in lateral and dorsal recumbency. Previous investigations have reported a large shunt fraction (Q_S/Q_T) in laterally recumbent anesthetized horses (Hall et al., 1968). These data suggest that true small airway closure is present in dependent lung units in laterally and dorsally recumbent horses.

The onset of phase IV has been correlated with the pressure-volume coordinates of the inflection point (P_{IP} , V_{IP}) of the lung P-V curve. In excised dog and monkey lungs, the pressure at CV (P_{CV}) and the pressure at the inflection point (P_{IP}) were strongly correlated (Glaister et al., 1973B). Ingram et al. (1974) reported a close agreement between CV and the volume at the inflection point (V_{IP}) in man. These correlations suggested that the inflection point of the P-V curve reflected the presence of small airway closure. However, Demedts et al. (1975) and Lai et al. (1977) did not find as strong a relationship between the P-V inflection point and the P-V coordinates at CV in man or dogs, and in general found V_{IP} to exceed CV. In this study, there was a significant correlation of P_{CV} on P_{IP} and CV on V_{IP} , but this relationship was not as strong as the correlation reported in the studies of Glaister or Ingram. Also, the coordinates of the P-V inflection

point were consistently greater than the P-V coordinates at the onset of phase IV.

The discrepency between investigations examining the relationship of the quasi-static P-V curve to the onset of phase IV may reflect species and interanimal differences in the regional P-V curve. shape of the regional P-V curve is determined by a combination of lungchest wall interactions, mechanical interdependence and regional surface tension forces. If the lung P-V curve is considered as a sum of individual regional P-V relationships the inflection point of the lung as a whole (dV/dP = maximum) occurs when a majority of individual units are also at their regional P-V inflection points. Glaister et al. (1973A) modelled the excised lung P-V curve as a rising exponential function. If regional P-V behavior follows this form, as regional pressure approaches 0 cm $\rm H_2^{0}$, the regional rate of volume change (dV/dP) approaches its maximum, i.e., the regional inflection point. At regional pressures below 0 cm H₂O, the unit is at its regional RV, and is effectively 'closed'. Therefore, the agreement between P_{CV} and P_{TP} would be expected since a majority of units reach their 'closing' pressure (regional pressure = 0 cm H_20) and regional inflection point simultaneously, forcing the onset of phase IV and an inflection point in the overall lung P-V curve. However, if regional P-V behavior takes on a more sigmoid shape, the maximal rate of regional volume change no longer occurs at regional RV. As a result, the lung P-V inflection point is no longer directly related to regional 'closure' and a dissociation between P_{IP} and P_{CV} , and V_{IP} and CV occurs. The data of Table 2 and

poor correlations of P_{CV} on P_{IP} , and CV on V_{IP} reveals this dissociation, such that the lung P-V inflection point cannot be used as an accurate predictor of small airway closure in horses.

The single breath N₂ washout also provides an index of the amount of regional inhomogeneities in lung emptying. The slope of phase III is determined by the magnitude of differences in regional concentration of a marker gas, and differences in regional emptying rates. Asynchronous lung emptying is significantly reduced in the sternally recumbent horse (slope phase III, Table 2). Similar changes in phase III with position are seen in man and dog, with the slope of phase III reduced in prone as compared to the lateral or supine postures (Cortese et al., 1976; Lai et al., 1977).

The major factor influencing asynchronous lung ventilation is the distribution of gravitational stresses within the lung (Anthonisen et al., 1970; Glaister et al., 1973B; Michels and West, 1977). Glazier et al. (1967) measured alveolar size in dog lungs frozen in situ in both upright and inverted animals. In upright dogs, there was a 4:1 vertical gradient in alveolar size from apex to base, while inverted dogs showed a uniform distribution of alveolar sizes. Regional distending force due to gravity in any plane taken through the lung normal to the gravitational field is proportional to the cross sectional area of the lung in the plane and the mass of lung below the plane. Measurements of cross sectional area and lung weights showed a large vertical gradient of regional distending force in the upright (anterior-posterior) dog lung, but only a small gradient in the inverted lung (Glazier et al.,

1967). These findings were due to the conical shape of the dog lung, with relatively more lung mass residing in the posterior regions.

The majority of the equine lung resides in the dorsal portion of the thorax (Getty, 1975). In sternal recumbency, as in the inverted dog, upper regions will have large cross sectional areas and tend to be distended by the bulk of the lung. Successively inferior regions will have smaller cross sections, but support proportionately less lung The net result will be a relatively homogenous distribution of gravitational stress throughout the lung as evidenced by the small slope to phase III (Table 2). With lateral and dorsal recumbency, the degree of asynchronous ventilation is increased. This increase in the slope of phase III reflects either an increase in regional N2 concentration differences or an alteration in the pattern of lung emptying. the pattern of lung emptying is similar between postures, increased regional stratification of N_2 must be involved. Regional filling will be influenced by the presence and amount of airway closure, with more closure causing greater regional differences in N2 concentration. Thus, the increased slope of phase III may be directly linked to an increased amount of small airway closure in the lateral and dorsal postures, supporting the evidence that small airway closure is present in the lateral and dorsal positions but reduced in sternal recumbency. Dynamic factors such as diaphragmatic contraction (Roussos et al., 1976) and thoracic muscle tone (Rehder et al., 1977) have been shown to alter intrapulmonary regional gas distributions and may also play a role in determining the slope of phase III in the different body positions.

Subdivisions of lung volume in the horse have not been well investigated. In anesthetized, suspended upright horses, FRC determined plethysmographically averaged 19 1, with an ER of 9 1 and VC of 33 1 (Leith and Gillespie, 1971). In the sternally recumbent horse in the present study, FRC measured by indicator dilution averaged 25 1, with an ER of 8 1 and VC of 36 1 (Tables 1 and 3). Functional residual capacity is determined by the equilibrium position of the lung and The weight of the horse on the sternum may cause dorso-ventral thorax. compression and lateral thoracic expansion, accounting for the larger FRC in the sternally recumbent animal over the suspended upright horse. Other factors that may also contribute to the difference in FRC between this study and the data of Leith and Gillespie are differences in recent lung volume history, in anesthetic agent, and in plane of anesthesia. Despite the elevated FRC, there is good agreement between ER and VC, indicating that the sternal position may closely approximate the standing animal. Further, since plethysmographic FRC, which measures total thoracic gas, is not markedly greater than the FRC from the N_{O} dilution method, which measures gas in communication with the mouth, there is apparently little trapped gas. This supports the conclusion that small airway closure may not be present during tidal breathing in the sternally recumbent horse.

Functional residual capacity is reduced by 50% in the lateral and dorsal postures as compared with awake standing or sternally recumbent animals (Table 3, McDonell and Hall, 1974). This may result from 1) a change in the equilibrium position of the lung and thorax, or 2) an

artifact due to a failure to measure gas trapped behind closed airways. Radiographs of the human and equine thorax in lateral recumbency show reductions in lung area due to compression of the down lung by the viscera and mediastinal structures (Nunn, 1969; McDonell, personal communication). In man, the change from seated to supine posture accounted for 60% of the reduction in FRC seen during anesthetia, with 40% occurring after induction of anesthesia (Craig et al., 1971A,B; Don et al., 1972). There was very little trapped gas in conscious subjects, and the increase in trapped gas with anesthesia represented less than a 10% artifact in the determination of FRC (Don et al., 1972).

Since FRC and ER were measured under different conditions and with a different population of horses, the extrapolation of absolute lung volumes from the two groups of horses must be cautioned (Figure 12). Although it appears that there is a large increase in RV in sternal posture, it is not possible to determine how much of this increase is artifactual. Because of the effects of lung volume history and P-V hysteresis on lung elastic recoil, FRC may correspond to any lung volume between RV and the resting lung volume on the deflation limb of the P-V curve. For this reason, comparison of RV, TLC, and the absolute lung volume at the onset of phase IV (closing capacity, CC) between positions is difficult. However, the effect of position on FRC, and estimates of RV, CC, and TLC probably reflects changes in regional stress distributions through the lung and lung-chest wall interactions in the different positions.

Regional inhomogeneities of lung volumes and tidal volumes were assessed by multiple breath open circuit N_2 washins. Three basic equations were solved by non-linear least squares minimization of the residuals (measured-predicted) to predict the N_2 dilution phenomena. The estimated FRC given by five models of the lung were compared with the FRC determined by closed circuit N_{γ} equilibration (Table 3). The incorporation of a deadspace volume ($V_{\rm D}$) was essential for accurate prediction of FRC. The three models accounting for $V_{\rm D}$, 1) two compartment with parallel, equal $V_{\rm D}$, 2) two compartment with common $V_{\rm D}$ (Weber and Bouhuys, 1959), and 3) continuous distribution of specific tidal volume (Gomez, 1963), are equivalent as judged by their ability to reduce the variance of residuals (Table 4). Mixed expired N2 concentration is apparently relatively insensitive to functional differences in lung clearance, pointing out a major problem in interpreting the results from the N₂ washin: identical mathematical equations may be interpreted in markedly different fashion (two compartment with and without $V_{\rm D}$), and very different mathematical formulations predict the data equally well (compartmental versus a continuous distribution). Due to this limitation, the significance of the volume and tidal volume estimates given in Table 5 is unclear. The models do however provide a means to accurately estimate FRC by monitoring F_{N_2} for 20 breaths without the necessity for a closed, leak proof system or the collection of all expired gas for a long period of time during a N_2 washout.

The distribution of ventilation in each position is given by the effective specific tidal volume (ξ), and represents the volume of fresh

gas (effective tidal volume, $V'_T = V_T - V_D$) delivered to the initial compartment volume with each breath (Table 6). The difference in predicted ξ between the common deadspace and parallel deadspace two compartment models is small and does not show an appreciable shift in distribution of the tidal volume with body position.

While the models employing two compartments give similar results, the common mixing chamber of the Weber-Bouhuys model is more anatomically correct. However, this model does not include a term for asynchronous lung filling and emptying, and assumes that each compartment receives a constant fraction of deadspace gas on inspiration. If asynchronous ventilation exists, the partitioning of deadspace gas will be altered, with the compartment leading inspiration making a greater contribution to deadspace gas concentration and also reinspiring a greater percentage of deadspace gas on the subsequent breath. The limit of this case would be two parallel units with the unit lagging inspiration not starting to inspire until all the deadspace gas was reinspired by the unit leading inspiration. This is equivalent to two independent compartments; one with deadspace equal to $\boldsymbol{V}_{\boldsymbol{D}}$ and the other with no deadspace. While the bulk distribution of ventilation determined by the N2 washin was unchanged with body position, the increased asynchronous ventilation in lateral and dorsal recumbency does indicate a shift in regional intrapulmonary gas distributions.

The model of Gomez (1963) attempts to solve the dilution function for a continuous distribution of specific tidal volumes, and is based on an extension of the two compartment model to an infinite number of parallel, equal volume units. Mean distributions of ξ predicted by this model are shown in Figure 11. Parameters of the distribution (mean, mode, half-width) have been used to evaluate changes in lung function (Filler and Gomez, 1966). In several horses, N_2 washins were predicted by distributions that approached their maximal value as ξ approached zero. This condition has been seen in obstructive lung disease (Gomez et al., 1964), and may reflect the addition of an airway closure component to the dilution function. In horses which did not exhibit this type of distribution, the half-width and mode were not a function of body position. This supports the compartmental model results, indicating no major shift in the pattern of ventilation with posture.

From these investigations, sternally recumbent anesthetized horses show respiratory system pressure-volume characteristics and subdivisions of lung volume similar to those in the upright animal. In the sternal position, there is only a small degree of asynchronous ventilation with the possibility of small airway closure occurring only at end-expiration. In lateral and dorsal recumbency, there is a 50% reduction in FRC, a decrease in VC, and an increase in asynchronous ventilation. The change in VC and reduction of ER below CV indicate the possibility of small airway closure occurring during tidal breathing. There was no significant change with position in the distribution of lung volume or tidal volume determined by the multiple breath N_2 washin. The increased asynchrony of ventilation and potential for small airway closure during tidal breathing may increase V/Q inequalities and be the predominant

factor involved in the increased alveolar-arterial $\mathbf{0}_2$ tension differences and intrapulmonary shunt associated with general anesthesia in the horse.



LIST OF REFERENCES

- Agostoni, E., E. D'Angelo, M. V. Bonanni. The effect of the abdomen on the vertical gradient of pleural surface pressure. Resp. Physiol. 8:332-346, 1970.
- Agostoni, E., E. D'Angelo. Topography of pleural surface pressure during simulation of gravity effect on abdomen. Resp. Physiol. 12:102-109, 1971.
- Anthonisen, N. R., J. Danson, P. C. Robertson, W. R. D. Ross. Airway closure as a function of age. Resp. Physiol. 8:58-65, 1969/70.
- Anthonisen, N. R., P. C. Robertson, W. R. D. Ross. Gravity dependent sequential emptying of lung regions. J. Appl. Physiol. 28:589-595, 1970.
- Bergman, N. A. Components of the alveolar-arterial oxygen tension difference in anesthetized man. Anesthesiology 28:517-527, 1967.
- Bergman, N. A. Pulmonary diffusing capacity and gas exchange during halothane anesthesia. Anesthesiology 32:317-324, 1970.
- Bevington, P. R. Data reduction and error analysis for the physical sciences. McGraw Hill, New York, 1969.
- Brown, E. S., R. P. Johnson, J. A. Clements. Pulmonary surface tension. J. Appl. Physiol. 14:717-720, 1959.
- Burger, E. J., P. Macklem. Airway closure: Demonstration by breathing 100% O₂ at low lung volumes and by N₂ washout. J. Appl. Physiol. 25:139-148, 1968.
- Campbell, E. J. M., J. F. Nunn, B. W. Peckett. A comparison of artificial ventilation and spontaneous respiration with particular reference to the ventilation-blood flow relationship. Br. J. Anaesth. 166-175, 1958.
- Clements, J. A., R. F. Hustead, R. P. Johnson, I. Gribetz. Pulmonary surface tension and alveolar stability. J. Appl. Physiol. 16:444-450, 1961.
- Cortese, D. A., J. R. Rodarte, K. Rehder, R. E. Hyatt. Effect of posture on the single-breath oxygen test in normal subjects.
 J. Appl. Physiol. 41:474-479, 1976.

- Craig, D. B., D. S. McCarthy. Airway closure and lung volumes during breathing with maintained airway positive pressures. Anesthesiology 36:540-543, 1972.
- Craig, D. B., W. M. Wahba, H. F. Don. Closing volume and its relationship to gas exchange in seated and supine positions. J. Appl. Physiol. 31:717-721, 1971A.
- Craig, D. B., W. M. Wahba, H. F. Don. Airway closure and lung volumes in surgical positions. Can. Anes. Soc. J. 18:92-98, 1971B.
- Darling, R. C., A. Cournand, D. W. Richards, Jr., B. Domanski. Studies on intrapulmonary mixture of gases. V. Forms of inadequate ventilation in normal and emphysematous lungs, analyzed by means of breathing pure oxygen. J. Clin. Invest. 23:55-67, 1944.
- Demedts, M., J. Clement, D. C. Stanescu, K. P. Van de Woestijne. Inflection point on transpulmonary pressure-volume curves and closing volume. J. Appl. Physiol. 38:228-235, 1975.
- Dollfus, R. E., J. Milic-Emili, D. V. Bates. Regional ventilation of the lung studied with boluses of 133 Xenon. Resp. Physiol. 2:234-246, 1967.
- Don, H. F., B. D. Craig, W. M. Wahba. The measurement of gas trapped in the lungs at functional residual capacity and the effects of posture. Anesthesiology 35:582-590, 1971.
- Don, H. F., W. M. Wahba, D. B. Craig. Airway closure, gas trapping, and the functional residual capacity during anesthesia.

 Anesthesiology 36:533-539, 1972.
- Engel, L. A., A. Grassino, N. R. Anthonisen. Demonstration of airway closure in man. J. Appl. Physiol. 38:1117-1125, 1975.
- Filler, J., D. Gomez. The continuous distribution of specific tidal volume throughout the lungs of children. Amer. Rev. Resp. Dis. 93:9-16, 1966.
- Fowler, W. S. Lung function studies. III. Uneven pulmonary ventilation in normal subjects and patients with pulmonary disease.

 J. Appl. Physiol. 2:283-299, 1949.
- Fowler, W. S., E. R. Cornish, S. S. Kety. Lung function studies. VIII.

 Analysis of alveolar ventilation by pulmonary N₂ clearance curves.

 J. Clin. Invest. 31:40-50, 1952.
- Fry, D. L. Theoretical considerations of the bronchial pressure flow volume relationship with particular reference to the maximum expiratory flow-volume curve. Phys. Med. Biol. 3:174-194, 1958.

- Getty, R. Anatomy of Domestic Animals. Vol. 1. W. B. Saunders Co., Philadelphia, 1975.
- Gillespie, J. R., W. S. Tyler, V. E. Eberly. Pulmonary ventilation and resistance in emphysematous and control horses. J. Appl. Physiol. 21:416-422, 1966.
- Gillespie, J. R., W. S. Tyler, L. W. Hall. Cardiopulmonary dysfunction in anesthetized, laterally recumbent horses. Am. J. Vet. Res. 30:61-72, 1969.
- Glaister, D. H., R. C. Schroter, M. F. Sudlow, J. Milic-Emili. Bulk elastic properties of excised lungs and the effect of a transpulmonary pressure gradient. Resp. Physiol. 17:347-364, 1973A.
- Glaister, D. H., R. C. Schroter, M. F. Sudlow, J. Milic-Emili.

 Transpulmonary pressure gradient and ventilation distribution in excised lung. Resp. Physiol. 17:365-385, 1973B.
- Glazier, J. B., M. B. Hughes, J. E. Maloney, J. B. West. Vertical gradient of alveolar size in lungs of dogs frozen intact. J. Appl. Physiol. 23:694-705, 1967.
- Gomez, D. A mathematical treatment of the distribution of tidal volume throughout the lung. Proc. Nat. Acad. Sci. U. S. 49:312-319, 1963.
- Gomez, D., W. A. Briscoe, G. Cumming. Continuous distribution of specific tidal volume throughout the lung. J. Appl. Physiol. 19:683-692, 1964.
- Gomez, D., J. Filler. On the continuous distribution of specific tidal volume throughout the lungs. Amer. Rev. Resp. Dis. 93:1-8, 1966.
- Hall, L. W., J. R. Gilespie, W. S. Tyler. Alveolar-arterial oxygen tension differences in anesthetized horses. Br. J. Anaesth. 40:560-567, 1968.
- Hashimoto, T., A. C. Young, C. J. Martin. Compartmental analysis of the distribution of gas in the lungs. J. Appl. Physiol. 23:203-209, 1967.
- Hyatt, R. E., G. C. Okeson, J. R. Rodarte. Influence of expiratory flow limitation on the pattern of lung emptying in normal man. J. Appl. Physiol. 35:411-419, 1973.
- Ingram, R. H., C. F. O'Cain, W. W. Fridy. Simultaneous quasi-static
 lung pressure-volume curves and "closing volume" measurements.
 J. Appl. Physiol. 36:135-141, 1974.

- Kaneko, K., J. Milic-Emili, M. B. Dolovich, A. Dawson, D. V. Bates.
 Regional distribution of ventilation and perfusion as a function of body position. J. Appl. Physiol. 21:767-777, 1966.
- Krueger, J. J., T. Bain, J. L. Patterson, Jr. Elevation gradient of intrathoracic pressure. J. Appl. Physiol. 16:465-468, 1961.
- Lai, Y., J. R. Rodarte, R. E. Hyatt. Effect of body position on lung emptying in recumbent anesthetized dogs. J. Appl. Physiol. 43:983-987, 1977.
- Leith, D. E., J. Mead. Mechanisms determining residual volume of the lungs in normal subjects. J. Appl. Physiol. 23:221-227, 1967.
- Leith, D. E., J. R. Gillespie. Respiratory mechanics of normal horses and one with chronic obstructive lung disease. Fed. Proc. 30:556, 1971.
- Macklem, P. T., J. Mead. Factors determining maximum expiratory flows in dogs. J. Appl. Physiol. 25:159-169, 1968.
- Marshall, B. E., P. J. Cohen, C. H. Klingenmaier. Pulmonary venous admixture before, during and after halothane-oxygen anesthesia in man. J. Appl. Physiol. 27:653-657, 1969.
- McDonell, W. N., L. W. Hall. Functional residual capacity in conscious and anesthetized horses. Brit. J. Anaesth. 46:802-803, 1974.
- Mead, J., T. Takishima, D. Leith. Stress distribution in lungs: a model of pulmonary elasticity. J. Appl. Physiol. 28:596-608, 1970.
- Mead, J., J. L. Whitenberger, E. P. Radford, Jr. Surface tension as a factor in pulmonary volume-pressure hysteresis. J. Appl. Physiol. 10:191-196, 1957.
- Mellemgaard, K. The alveolar-arterial oxygen tension difference: its size and components in normal man. Acta Physiol. Scand. 67:10-20, 1966.
- Michels, D. B., J. B. West. Pulmonary function during short periods of zero gravity. Fed. Proc. 36:468, 1977.
- Milic-Emili, J., A. M. Henderson, M. B. Dolovich, D. Trop, K. Kaneko. Regional distribution of inspired gas in the lung. J. Appl. Physiol. 21:749-759, 1966.
- Murphy, B. G., L. A. Engel. Model of the human lung pressure volume curve. Fed. Proc. 36:468, 1977.

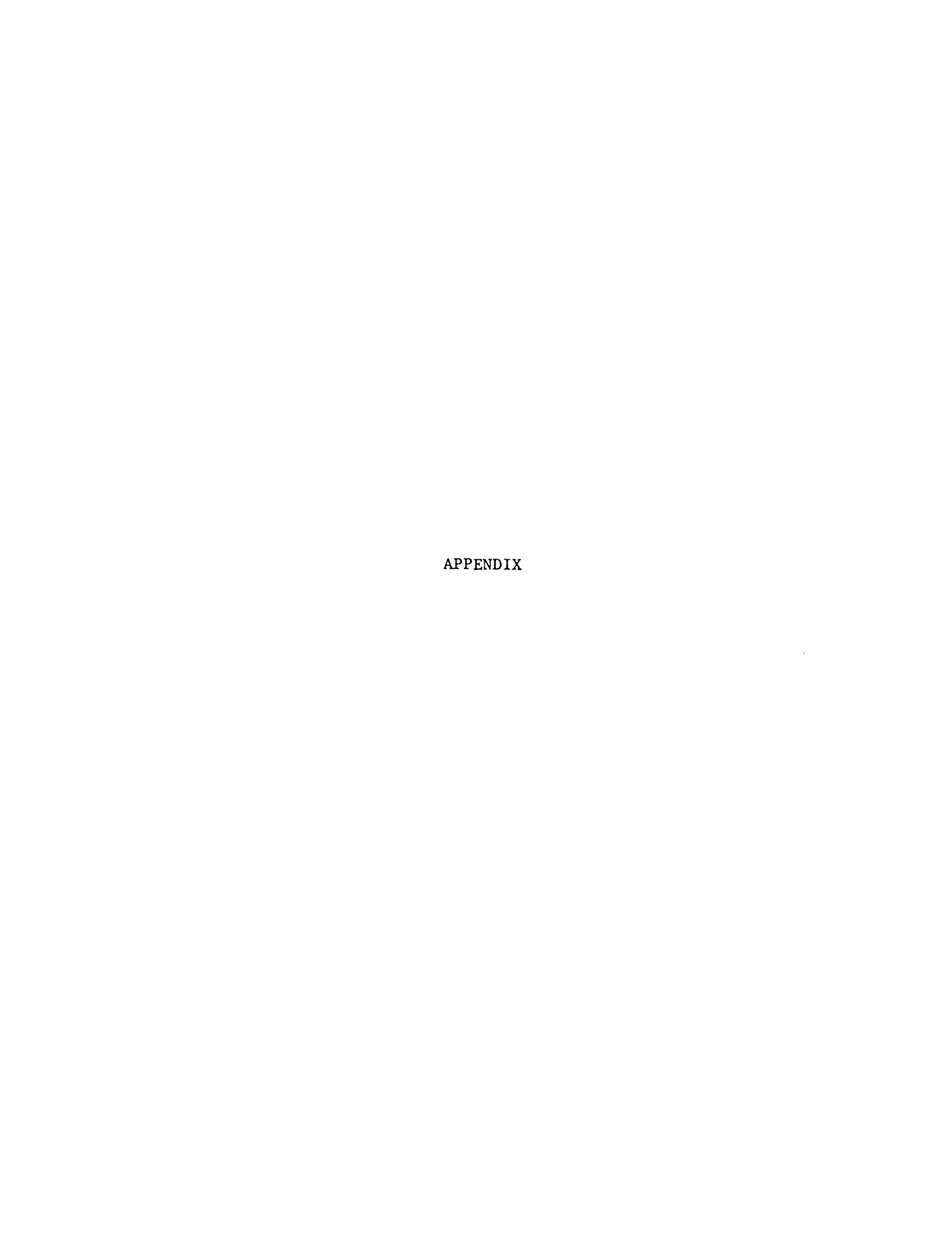
- Nakamura, T., T. Takishima, T. Okubo, T. Sasaki, H. Takahashi.

 Distribution function of the clearance time constant in lungs.

 J. Appl. Physiol. 21:227-232, 1966.
- Nunn, J. F. Factors influencing the arterial oxygen tension during halothane anesthesia with spontaneous respiration. Brit. J. Anaesth. 36:327-341, 1964.
- Nunn, J. F. Applied Respiratory Physiology. Butterworth and Co., London, 1969.
- Nunn, J. F., N. A. Bergman, A. J. Gleman. Factors influencing the arterial oxygen tension during anesthesia with artificial ventilation. Brit. J. Anaesth. 37:898-914, 1965.
- Okubo, T., C. Lanfant. Distribution function of lung volume and ventilation determined by lung N₂ washout. J. Appl. Physiol. 24:658-667, 1968.
- Raine, J. M., J. M. Bishop. A-a difference in O₂ tension and physiological deadspace in normal man. J. Appl. Physiol. 18:284-288, 1963.
- Rehder, K., A. D. Sessler, J. R. Rodarte. Regional intrapulmonary gas distribution in awake and anesthetized-paralyzed man. J. Appl. Physiol. 42:391-402, 1977.
- Rodarte, J. R., R. E. Hyatt, D. A. Cortese. Influence of expiratory flow and closing capacity at low expiratory flow rates. J. Appl. Physiol. 39:60-65, 1975.
- Rohlf, F. J., R. R. Sokal. Statistical Tables. W. H. Freeman and Co., San Francisco, 1969.
- Roussos, C. S., D. I. M. Siegler, L. A. Engel. Influence of diaphragmatic contraction and expiratory flow on the pattern of lung emptying. Resp. Physiol. 27:157-167, 1976.
- Roussos, C. S., R. R. Martin, L. A. Engel. Diaphragmatic contraction and the gradient of alveolar expansion in the lateral posture. J. Appl. Physiol. 43:32-38, 1977.
- Sokal, R. R., F. J. Rohlf. Biometry. W. H. Freeman and Co., San Francisco, 1969.
- Travis, D. M., M. M. Green, H. F. Don. Expiratory flow rate and closing volumes. J. Appl. Physiol. 35:626-630, 1973.

1
]
<u> </u>
,
i
į į

- Weber, J., A. Bouhuys. Theoretical considerations on lung clearance. Acta Physiol. Pharmacol. Neerlandica 8:121-136, 1959.
- Wyche, M. Q., R. L. Teichner, T. Kallos, B. E. Marshall, T. C. Smith. Effects of continuous positive pressure breathing on functional residual capacity and arterial oxygenation during intraabdominal operations. Anesthesiology 38:68-74, 1973.



APPENDIX

The quantity of nitrogen (Q $_{\mbox{\scriptsize N}_2}$) in a single, well-mixed compartment at any breath n is given by:

$$Q_{N_2} = F_{N_2}(n) \cdot V \tag{11}$$

where:

 F_{N_2} = fractional N_2 concentration at breath n_2 V = volume of compartment

Following inspiration of a tidal volume (V_T) with $F_{IN_2} = 0$, the nitrogen concentration on the subsequent expiration is given by:

$$F_{N_2}(n+1) = F_{N_2}(n) \left[\frac{V}{V+V_T} \right]$$
 (1)

In general, the dilution function obeys:

$$F_{N_2}(n) = F_{N_2}(0) \left[\frac{V}{V+V_T} \right]^n$$
 (12)

When inspired nitrogen concentration (F_{IN_2}) is not zero:

$$F_{N_2}(n+1) = \frac{F_{N_2}(n) \cdot v + F_{IN_2} \cdot v_T}{v + v_T}$$
 (13)

Since F = F (∞), substituting F (∞) for F and subtracting F (∞) from both sides of the equation yields:

$$F_{N_2}(n+1) - F_{N_2}(\infty) = \left[F_{N_2}(n) - F_{N_2}(\infty)\right] \left[\frac{V}{V+V_T}\right]$$
 (14)

Expressing F_{N_2} as a dimensionless N_2 concentration (F'_{N_2}) , F'_{N_2} (n) at any breath n is then given in general form by:

$$F'_{N_{2}}(n) = \frac{F_{N_{2}}(n) - F_{N_{2}}(\infty)}{F_{N_{2}}(0) - F_{N_{2}}(\infty)} = \left[\frac{V}{V+V_{T}}\right]^{n}$$
(2)

Extending equation 2 to k parallel, independent compartments, the dilution of each compartment i is given by equation 1 and contributes $F_{i_{N_{2}}}(n) \cdot V_{T} \text{ nitrogen to the expirate (equation 11). The total quantity of }_{N_{2}}^{N_{2}}(n) \cdot V_{T}^{N_{3}}(n) \cdot V_{T}^{N_$

$$Q_{totN_2}(n) = \sum_{i=1}^{k} F_{i}(n) \cdot V_{T_i}$$
(15)

and mean expired $F_{N_2}(n)$ will be:

$$F_{N_2}(n) = \frac{Q_{totN_2}(n)}{V_T}$$
 (16)

where:

$$\mathbf{v_T} = \begin{array}{c} \mathbf{k} \\ \Sigma \\ \mathbf{i} = 1 \end{array} \quad \mathbf{v_T_i}$$

Assuming all k compartments start at the same initial condition, and substituting for $Q_{\text{tot}N_2}(n)$ and $F_{\text{i}N_2}(n)$, the dilution in terms of the dimensionless expired nitrogen concentration follows:

$$F'_{N_2}(n) = \frac{1}{V_T} \quad \sum_{i=1}^k V_{T_i} \left[\frac{V_i}{V_i + V_{T_i}} \right]^n$$
(3)

The addition of a deadspace volume $(V_{\stackrel{}{D}})$ to the single compartment model yields:

$$F_{N_2}(n+1) = F_{N_2}(n) \left[\frac{v + v_D}{v + v_T} \right]$$
 (17)

Where F_{N_2} (n) now represents the N_2 concentration in the compartment, or end tidal F_{N_2} , and not mean expired F_{N_2} . It follows:

$$F'_{N_2}(n) = \left[\frac{v + v_D}{v + v_T}\right]^n \tag{4}$$

When extending this model to k independent compartments with parallel deadspaces (V_{D_i}), the mixed expired F_{N_2} (n) can be defined several ways. By summing the quantity of N_2 contributed by each compartment, the total expired N_2 is,

$$Q_{totN_2}(n) = \sum_{i=1}^{k} F_{i}(n) \cdot (V_{T_i} - V_{D_i})$$
 (18)

By dividing $Q_{\text{tot}N_2}$ by V_T , the mean expired F_{N_2} is obtained. However, it is convenient to simply measure an average 'alveolar' concentration, neglecting the initial deadspace gas contribution to mean expired F_{N_2} . Average 'alveolar' or end tidal F_{N_2} (n) is given by:

$$F_{N_2}(n) = \frac{1}{V_T - V_D} \sum_{i=1}^{k} F_{i}_{N_2}(n) (V_T - V_D)$$
 (19)

where:

$$V_{T} = \begin{array}{c} k \\ \Sigma \\ i=1 \end{array} \qquad V_{T}$$

$$V_{D} = \begin{array}{c} k \\ \Sigma \\ i=1 \end{array} \qquad V_{D}$$

Substituting F' $_{N_2}$ (n) from the single compartment case for F $_{i_{N_2}}$ (n), the dimensionless mixed end tidal F $_{N_2}$ will be:

$$F'_{N_{2}}(n) = \frac{1}{V_{T} - V_{D}} \sum_{i=1}^{k} (V_{T_{i}} - V_{D_{i}}) \left[\frac{V_{i} + V_{D_{i}}}{V_{i} + V_{T_{i}}} \right]^{n}$$
 (20)

The two compartment case in the presence of a common V_D has been developed by Weber and Bouhuys (1959). Each compartment is assumed to contribute a constant fraction to the deadspace gas $(F_{D_{N_2}})$ on expiration:

$$F_{DN_2}(n) = \frac{V_{T_1}}{V_T} F_{1N_2}(n) + \frac{V_{T_2}}{V_T} F_{2N_2}(n)$$
 (21)

At the n+l inspiration, the two compartments receive a fraction of gas at $F_{D_{N_2}}(n)$ with the remainder of the inspirate at $F_{N_2}=0$. The quantity of gas at end inspiration in either compartment is the quantity at expiration n plus the fraction of deadspace gas reinhaled:

$$F_{1_{N_{2}}}(n+1) \cdot (V_{T_{i}} + V_{i}) = F_{1_{N_{2}}}(n) \cdot V_{i} + F_{D_{N_{2}}}(n) \frac{V_{T_{i}} \cdot V_{D}}{V_{T}}; i=1,2$$
 (22)

and:

$$V_T = V_{T_1} + V_{T_2}$$

Solving for $F_{i_{N_2}}$ (n + 1) and substituting for $F_{D_{N_2}}$ (n):

$$F_{1_{N_2}}(n+1) = k_0 F_{1_{N_2}}(n) + m_0 F_{2_{N_2}}(n)$$
 (23)

$$F_{2N_2}(n+1) = P_0 F_{1N_2}(n) + q_0 F_{2N_2}(n)$$
 (24)

where:

$$k_{o} = \frac{v_{1} + \left(\frac{v_{T_{1}}}{v_{T}}\right)^{2} v_{D}}{v_{1} + v_{T_{1}}}$$

$$m_{o} = \frac{\left(\frac{v_{T_{1}}}{v_{T}}\right)\left(\frac{v_{T_{2}}}{v_{T}}\right) v_{D}}{v_{1} + v_{T_{1}}}$$

$$p_{o} = \frac{\left(\frac{v_{T_{1}}}{v_{T}}\right)\left(\frac{v_{T_{2}}}{v_{T}}\right) v_{D}}{v_{2} + v_{T_{2}}}$$

$$q_{o} = \frac{v_{2} + \left(\frac{v_{T_{2}}}{v_{T}}\right)^{2} v_{D}}{v_{2} + v_{T_{2}}}$$

In matrix form the general solution can be shown to be:

$$\begin{pmatrix} F_{1_{N_{2}}}(n) \\ F_{2_{N_{2}}}(n) \end{pmatrix} = \begin{pmatrix} k_{o} & m_{o} \\ p_{o} & q_{o} \end{pmatrix} \begin{pmatrix} F_{1_{N_{2}}}(0) \\ F_{2_{N_{2}}}(0) \end{pmatrix}$$
(25)

The solution for the dimensionless end tidal N_2 concentration $(F'_{N_2} = F_{D_{N_2}})$ follows:

$$F'_{N_2}(n) = \begin{pmatrix} v_{T_1} & v_{T_2} \\ v_{T} & v_{T} \end{pmatrix} \begin{pmatrix} k_0 & m_0 \\ p_0 & q_0 \end{pmatrix}^n \begin{pmatrix} 1 \\ 1 \end{pmatrix}$$
 (5)

The distribution of specific tidal volume (ξ) model of Gomez (1963) arises from the general k compartment model with each compartment having the same initial volume (V_O):

$$\xi_{i} = V_{T_{i}}/V_{o}$$

$$F'_{N_{2}}(n) = \frac{1}{V_{T}} \sum_{i=1}^{k} V_{T_{i}} \frac{V_{o}}{V_{o} + V_{T_{i}}} = \frac{V_{o}}{V_{T}} \sum_{i=1}^{k} \frac{\xi_{i}}{(1 + \xi_{i})^{n}}$$
(26)

By allowing $k \neq \infty$ and $V_0 \neq 0$, ξ_1 becomes a continuous variable ξ and yields a linear integral equation with $f(\xi)$ defining the distribution function of ξ :

$$F'_{N_2}(n) = \frac{V_o}{V_T} \int_{\xi_1}^{\xi_2} \frac{\xi + (\xi)}{(1 + \xi)^n} d\xi$$
 (27)

The solution for $f(\xi)$ requires evaluating the inverse Laplace transform of F'_{N_2} (n). Gomez and Filler (1966) proposed approximating the washout function by the empirical equation:

$$F'_{N_2}(n) = \frac{1}{(1 + a \cdot n)^2}$$
 (6)

where:

a,z = empirical constants

After determining a and z, the inverse Laplace transform and normalizing coefficients may be evaluated to yield V_0/V $f(\xi)$ (relative number of units) such that the area under the distribution is unity (notation of Gomez, 1963):

$$\frac{V_{o}}{V} f(\xi) = \mathcal{A} \frac{\ln(1+\xi)^{z-1}}{\xi(1+\xi)^{\alpha}}$$
 (28)

where:

$$\alpha = \frac{1}{a} + 1$$

$$\mathcal{A} = \frac{1}{\Gamma(z) \sum_{i=1}^{\infty} \frac{1}{(a+i)^{2}}}$$

 $\Gamma(z)$ = gamma function of z

and the mean of the distribution $(\overline{\xi}\,,\,V_{\overline{1}}/V)$ is given by:

$$\overline{\xi} = \frac{\Gamma(z) \mathcal{Q}}{(\alpha - 1)^2}$$
 (29)

